

Driving quantum systems with periodic conditional measurements

Quancheng Liu^{1,*}, Klaus Ziegler^{2,†}, David A. Kessler^{3,‡} and Eli Barkai^{1,§}

¹*Department of Physics, Institute of Nanotechnology and Advanced Materials, Bar-Ilan University, Ramat-Gan 52900, Israel*

²*Institut für Physik, Universität Augsburg, D-86135 Augsburg, Germany*

³*Department of Physics, Bar-Ilan University, Ramat-Gan 52900, Israel*



(Received 23 April 2021; accepted 5 April 2022; published 17 May 2022)

We consider the effect of periodic conditional no-click measurements on a quantum system. What is the final state of such a driven system? When the system has some symmetry built into it, the final state is a dark state provided that the initial state overlaps with this nondetectable fragment of the Hilbert space. We find two classes of such states: generic dark states that are found also for nonperiodic measurements, and Floquet dark states that are directly controlled by the periodicity of the measurements and which do not rely on the underlying symmetry of the Hamiltonian. A different behavior is found in the absence of dark manifolds, where for specific periodicities of the measurements we find nontrivial oscillatory dynamics, controlled by the measurement rate. Finally, when the control parameters are tuned, the eigenvalues of the survival operator coalesce to zero, and then one finds exceptional points with a large degeneracy. The physical meaning of this special type of degeneracy is that the null measurement process becomes impossible, implying that detecting the state is guaranteed. We analyze these effects with a nonperturbative method based on a classical charge picture.

DOI: [10.1103/PhysRevResearch.4.023129](https://doi.org/10.1103/PhysRevResearch.4.023129)

I. INTRODUCTION

The control of quantum systems is an extensively studied topic [1–6] which is essential for many areas of physics ranging from nuclear-magnetic-resonance experiments [7] to trapped ions [8,9], quantum optics [10], superconducting qubits [11], and quantum computing [12]. This can be done for molecular processes with laser pulses [13] that modify the system’s Hamiltonian or in condensed matter systems via advanced Floquet engineering [14–16]. Another option is to use measurements to drive quantum systems [17–29]. For example, dark-state engineering is used to drive systems to a desired steady state [30,31]. The general theme is to build a measurement protocol that drives a system to a particular final state.

Here, we consider quantum control of a generic quantum system with repeated conditional *null* measurements (see Fig. 1). Similar to the experimentally demonstrated approach in [32], we choose the set of measurements such that the system is not detected, also called no-click or postselection measurement [33–38]. However, the crucial difference is that in our study the measurements are made periodically. The

possibility of implementing our protocol in the laboratory is also made possible with the noise intermediate scale quantum hardware [39,40], for instance, the quantum computers from IBM [41] or Honeywell [42], where conditional projective measurement is realized as a designed quantum “IF” gate. Similar to periodic driving with an external force [43], in our protocol the measurements are performed stroboscopically. In essence, this replaces the repeated action of a force with a periodic action of a measurement. Our goal is to study the effect of periodic no-click measurements on a quantum system and explore the consequences of this type of dynamics which clearly differs from the widely studied periodic driving with a force field. A list of the main effects we find is presented in the summary of our paper, where we report six generic cases for the final state of the system.

Formally, the heart of our analysis is related to a non-Hermitian operator describing the combined effect of unitary evolution and measurement in one period. In general, non-Hermitian approaches [33,36,44–46] usually describe decay, namely, a continuous leakage of probability out of a quantum system, for example, describing photon emission, as is known from the quantum jump method in quantum optics [30,47] or the Lindblad approach to dissipation [48,49]. Our approach is different, as aside from a periodic measurement that collapses the wave function at the detection state suddenly, the evolution is purely unitary. Technically, this means that we must invoke a nonperturbative approach, and this challenge is met with a classical charge theory promoted by Grünbaum *et al.* [50,51]. Our work is also related to the study of Floquet physics in non-Hermitian systems [52,53], where a periodic drive is applied. In a broad sense, these investigations are related to our work, namely, if we consider the combined effects of unitary evolution and the measurement in one period as an effective

*qcliu.ac@gmail.com

†klaus.ziegler@physik.uni-augsburg.de

‡kessler@dave.ph.biu.ac.il

§Eli.Barkai@biu.ac.il

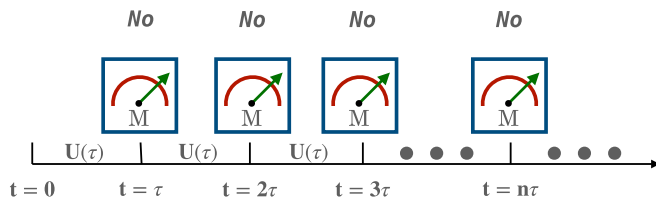


FIG. 1. Schematic depiction of the quantum driving via null detections. The quantum system is initially prepared at some pure state. Local measurements of a target state $|\psi_d\rangle$ are performed at discrete times $t = \tau, 2\tau, \dots, n\tau, \dots$, whose outcomes are postselected to null. We investigate the state of the quantum system under such repeated steering.

non-Hermitian action, then the periodic measurement process can be regarded as Floquet non-Hermitian operations. The unique part in this work is that the non-Hermitian action is induced by a *conditioned* projective measurement, which is sharp and discontinuous as we discussed above.

We explore a wide range of scenarios. First, we investigate dark-state physics. The Hilbert space under repeated measurements is fragmented, and two subspaces are created: one is called dark and the other bright. This mimics the effect of nonergodicity in classical systems and it is deeply related to many-body dark states [54]. A generic initial condition can belong to both subspaces. The conditional null measurements will drive the system to the dark subspace, which is fully characterized below. Interestingly, we find two classes of dark states. One type is called generic as these are states that can be found for nonperiodic measurements [55], and these arise from the symmetry of the Hamiltonian H . But, in addition to those, we find what we call Floquet dark states that are inherently related to the periodic driving and do not demand an *a priori* symmetry of H . This in turn implies that with periodic driving we may engineer dark states, for practically any system.

We then consider cases where the dark states do not exist, namely, we choose the period of driving far from the regime where Floquet dark states are obtained. Still, the system is driven to a final state, be it a fixed steady state or a time-dependent one. Here, the mentioned classical charge theory is again powerful as with it we obtain insights on these final states. The measurements can also drive the system to periodically oscillate in time, even for relatively large systems. This is promising for quantum control. Furthermore, measurement-based control is also flexible. For instance, one can easily modify the oscillation by changing the period of measurements. Finally, there are special cases where the conditional driving completely fails, and this is related to exceptional points [36,45,56–64] of the problem. The symmetry we find in the classical charge theory allows us to classify this special class of dynamics and predict where it is found in parameter space. In an engineering sense, working close to these degenerate states means that no-click measurements and hence control are not possible, but physically these points seem profound to us as the system exhibits there a gigantic degeneracy.

We also note there are also other protocols that realize quantum control with measurements, like the quantum Zeno

dynamics [65,66], using fast and multidimensional measurements [67]. Here we show that quantum control is possible without going to the Zeno regime, which is based on a clever choice of the measurement rate. We can efficiently control the quantum system with many fewer measurements and drive it to a deterministic final state. On the other hand, for the quantum Zeno dynamics, the evolution is unitary on the quantum Zeno subspace, which is defined by the multidimensional fast measurements. Hence, the non-Hermitian effects as we show here are also impossible to achieve by the quantum Zeno control since they explicitly depend on the rate of measurements. Note that the Zeno regime is a special case of our problem, and we derive a lower bound for the evolution time to drive the system, which is much slower if compared with the cases that are far from this limit (see Fig. 4, for example). The challenge is therefore to drive the system far from the well-studied case of Zeno.

The paper is organized as follows. Sections II and III give the model, general discussion of the mathematical properties of the survival operator, a mapping of the quantum problem to classical charge theory, and a simple discussion of the exceptional points. In Secs. IV and V we present the main results, namely, the state function under conditional measurements, for both finite and infinite measurement times. In Secs. VI and VII, we present three examples: a three-level system, an artificial atom that can shelve, and a glued binary tree with degeneracy. In Sec. VIII, we present general insights on the final state of the system with a perturbation approach. Then in Sec. IX, we discuss exceptional points in a more general setting from the point of view of the symmetry of the charge configuration. We close the paper with a summary in Sec. X.

II. SURVIVAL OPERATOR

As mentioned, we are interested in the evolution of the wave function of a system conditioned on null measurements. The model describes unitary dynamics interleaved with measurements. The system is discrete and finite, and H is the Hamiltonian, which governs the dynamics between measurement events. At the times $\tau, 2\tau, 3\tau, \dots$ we perform measurements in an attempt to detect the system in the target state $|\psi_d\rangle$. For example, for a tight-binding quantum walk on a tree (see Fig. 7), discussed below, $|\psi_d\rangle$ describes a localized node on the graph, or $|\psi_d\rangle$ can be an energy level (see Fig. 5), etc. τ is a free parameter. The outcome of a given measurement, at least in principle, is either the system is detected at the target state $|\psi_d\rangle$ or not. We condition the measurements and consider only the realization of the process described by the string: no, no, \dots , no, which repeats n times, namely, the particle has never been found in the target state, e.g., the quantum walker has not been detected on the specified node of the graph [68].

Therefore, the wave function after the first measurement is $|\psi_1\rangle = N_1(\mathbb{1} - D)\hat{U}(\tau)|\psi_{in}\rangle$. Here, $D = |\psi_d\rangle\langle\psi_d|$ is the projection operator onto the measured state, while $\hat{U}(\tau) = \exp(-iH\tau)$ is the unitary evolution operator, and we have set $\hbar = 1$. The operator

$$\hat{\mathbb{G}} = (\mathbb{1} - D)\hat{U}(\tau) \quad (1)$$

incorporates the unitary evolution in the time interval τ followed by the projection described by $\mathbb{1} - D$. The latter, when acting on the state function, wipes out the amplitude on the detected state, as the result of the measurement is null. The operator $\hat{\mathcal{S}}$ is called the survival operator as it describes the wave function that survives the detection (if the particle had been detected, the wave function would have collapsed on $|\psi_d\rangle$). Clearly, it is a nonunitary operator. Immediately after the n th measurement, the wave function $|\psi_n\rangle$ reads as

$$|\psi_n\rangle = N_n \hat{\mathcal{S}}^n |\psi_{in}\rangle. \tag{2}$$

Below we suppress the index n in the normalization N_n .

We are interested in the large- n limit. In this limit, we encounter a variety of dynamical features explored below. In one case, the dynamics is determined by a subset of energy levels, in another by a fixed point where the system has no dynamics at all. Finally, we observe oscillatory behavior; however, unlike the first case scenario, the eigenvalues determining this behavior are not standard energy levels of H . They are controlled by H , D , and τ . Our goal is to classify these behaviors and see when they emerge. What is clear is that the large- n limit is described by the set of eigenvalues of $\hat{\mathcal{S}}$ of largest magnitude; hence, this is what we study next.

As usual, since the operator $\hat{\mathcal{S}}$ is non-Hermitian it has left and right eigenvalues and eigenvectors and these are denoted

$$\hat{\mathcal{S}}|\xi^R\rangle = \xi|\xi^R\rangle, \quad \langle \xi^L | \hat{\mathcal{S}} = \langle \xi^L | \xi. \tag{3}$$

Here we used the fact, well known from linear algebra, that the left and right eigenvalues are equal; hence, they are denoted with ξ . These are complex numbers, and for the problem at hand, it was shown that these eigenvalues are all on the unit disk $|\xi| \leq 1$ [55,69]. We will use normalized states $\langle \xi^L | \xi^R \rangle = \langle \xi^L | \xi^L \rangle = 1$.

We start the analysis by considering three types of eigenvalues. The case $\xi = 0$, the case $0 < |\xi| < 1$, and then $|\xi| = 1$. When the eigenvalue is zero, we have

$$|\xi^R\rangle = \hat{U}^{-1}|\psi_d\rangle, \quad \langle \xi^L | = \langle \psi_d |, \tag{4}$$

which is obvious due to $(\mathbb{1} - D)U U^{-1}|\psi_d\rangle = 0$ and $\langle \psi_d | (\mathbb{1} - D) = 0$. The physical meaning of the $|\xi^R\rangle$ state is clear, as it is a state that is detected with probability one in the first measurement attempt. In fact, if we start in this state, namely, $|\psi_{in}\rangle = U^{-1}|\psi_d\rangle$, we cannot achieve the desired conditional measurement since the first measurement is always successful. This implies that not all initial conditions can yield a string of n null measurements, an issue we will return to below.

More interesting are the states with eigenvalues $|\xi| = 1$ on the unit circle. This set can be empty as we show below, but for now we assume that such states exist. These right eigenstates satisfy

$$\hat{\mathcal{S}}|\xi^R\rangle = \underbrace{\exp(i\theta)}_{\xi} |\xi_R\rangle. \tag{5}$$

We express these states in terms of linear combinations of stationary states of the time-independent Hamiltonian H . For that, we denote $H|E_{k,l}\rangle = E_k|E_{k,l}\rangle$, where k is the index of the distinct energy levels, while l is a quantum number denoting the degenerate sublevels, so that $l = 1, \dots, g_k$, where g_k is

the degeneracy of the energy level E_k . Degeneracy and hence symmetry play a crucial role here.

An obvious eigenstate of $\hat{\mathcal{S}}$ is an energy state $|E_{k,l}\rangle$ which is orthogonal with respect to the detected state, namely, if we have in our system a state $\langle \psi_d | E_{k,l} \rangle = 0$ we get

$$(\mathbb{1} - D)\hat{U}(\tau)|E_{k,l}\rangle = \exp(-iE_k\tau)|E_{k,l}\rangle. \tag{6}$$

Hence, all energy states which are orthogonal to the detected state are right eigenvectors of the survival operator $|\xi^R\rangle = |E_{k,l}\rangle$ with an eigenvalue $\xi = \exp(-iE_k\tau)$. Physically, this state corresponds to a dark state [30,55,70]. Namely, if such a state exists, and if it is chosen as the initial condition, it will never be detected. So, in this case, the condition of null measurements is guaranteed from the start. Similarly, it is easy to see that under the same condition, i.e., $\langle \psi_d | E_{k,l} \rangle = 0$, the corresponding left eigenvector is $\langle \xi^L | = \langle E_{k,l} |$. We see in this special example a property which is unique to states with eigenvalues on the unit circle, namely, $|\xi^L\rangle = |\xi^R\rangle$. This feature is of some importance later.

Our goal now is to consider other dark states, that are eigenstates of the survival operator, with eigenvalues on the unit circle. Recall that such states obviously have the largest possible eigenvalue and hence dominate the large- n limit, if they exist. We use the energy representation and consider a degenerate subspace in the Hilbert space, namely, $\{|E_{k,1}\rangle, \dots, |E_{k,g_k}\rangle\}$, where all these states have the same energy E_k . If some of them satisfy $\langle \psi_d | E_{k,l} \rangle = 0$ they are clearly dark as we have just explained. Consider now a linear combination of two energy states and we index these with $l = 1$ and 2 . We then find the eigenvector of $\hat{\mathcal{S}}$:

$$|\xi^R\rangle = N(\langle \psi_d | E_{k,2} \rangle |E_{k,1}\rangle - \langle \psi_d | E_{k,1} \rangle |E_{k,2}\rangle). \tag{7}$$

Here clearly $\hat{\mathcal{S}}|\xi^R\rangle = \exp(-iE_k\tau)|\xi^R\rangle$ since $U|\xi^R\rangle = \exp(-iE_k\tau)|\xi^R\rangle$ and $D|\xi^R\rangle = 0$, and so the eigenvalue of the survival operator is $\xi = \exp(-iE_k\tau)$, namely, it is just a phase determined by the energy E_k . Similarly, it is easy to see that $\langle \xi^L | = \langle \xi^R |$ is a left eigenvector of the survival operator, and hence $\langle \xi^L | \xi^R \rangle = 1$. So these vectors are parallel, unlike the left and right vectors we found above with zero eigenvalue $\xi = 0$ (and unlike the eigenvectors we discuss below with $|\xi| < 1$). The state in Eq. (7) is clearly dark in the sense that if we start in this state, the amplitude on the detected state is always zero. This, in turn, is because this is a stationary state of H , hence between measurements, the dynamics do not allow the leakage of probability amplitude to the detected state, so we never detect the system. Once again, by a dark state, we mean that even if we do not condition the measurements to be null, the sequence of measurements will never detect the particle.

We can easily construct other normalized dark states using similar methods. We denote these states, i.e., states that cannot be detected as $|\delta_{k,m}\rangle$ (δ is for dark). Following [55], we find that in an energy subspace with g_k states, there are $g_k - 1$ dark states $\{|\delta_{k,m}\rangle\}$ with $m = 1, \dots, g_k - 1$. These states are given by a Gram-Schmidt procedure [55,70]

$$|\delta_{k,m}\rangle = N \sum_{j=1}^m [|\alpha_{k,j}\rangle^2 |E_{k,m+1}\rangle - \alpha_{k,m+1}^* \alpha_{k,j} |E_{k,j}\rangle], \tag{8}$$

where $\alpha_{k,m} = \langle E_{k,m} | \psi_d \rangle$ and m goes from 1 to $g_k - 1$. All these states are orthonormal with respect to each other, and again they are stationary states of the system, namely, $H|\delta_{k,m}\rangle = E_k|\delta_{k,m}\rangle$. It is easy to see that these states are eigenstates of the survival operator with eigenvalue $\xi = \exp(-iE_k\tau)$, namely, these eigenvalues all fall on the unit circle since $\hat{\mathcal{C}}|\delta_{k,m}\rangle = \exp(-iE_k\tau)|\delta_{k,m}\rangle$. It is also easy to show that the left eigenvectors satisfy $\langle \xi^L | = \langle \xi^R |$.

Interestingly, there exists another class of dark states that are related to the periodicity of the measurements. These dark states, which we call Floquet dark states, arise when we tune the sampling time τ , such that the condition

$$(E_k - E_l)\tau = 0 \pmod{2\pi} \quad (9)$$

is satisfied, where $E_k \neq E_l$. The energy levels E_k and E_l are thus quasidegenerate for this particular τ . Consider two such energy states $|E_k\rangle$ and $|E_l\rangle$, and assume that these states are nondegenerate. Then consider their linear combination

$$|\delta\rangle = N(\langle \psi_d | E_l \rangle |E_k\rangle - \langle \psi_d | E_k \rangle |E_l\rangle). \quad (10)$$

This state is dark since after each period the amplitude on the detected state is zero.

Now we can consider a more general case, where the energy levels E_k and E_l are also degenerate. We can construct new dark states in the subspace $\{|E_{k,1}\rangle, \dots, |E_{k,g_k}\rangle, |E_{l,1}\rangle, \dots, |E_{l,g_l}\rangle\}$. Formally, this can be done by re-labeling the energy states $|E_{l,1}\rangle \rightarrow |E_{k,g_k+1}\rangle, \dots, |E_{l,g_l}\rangle \rightarrow |E_{k,g_k+g_l}\rangle$, then Eq. (8) can be applied again.

More importantly, with Eq. (9) we can construct a dark state in a nondegenerate system. Since such dark state is defined by the measurements, and more specifically by the period τ , this allows us to drive a system into a dark state independent of the symmetry of the specific system. This is a different route to perform the dark-state engineering for nondegenerate systems. In Secs. VIII B and VIII C we develop the charge theory to explore the physical effects close to the quasidegeneracy defined by Eq. (9).

We have seen how dark states can be presented as energy eigenstates of H but also as eigenstates of the survival operator $\hat{\mathcal{C}}$. The moduli of the corresponding eigenvalues of $\hat{\mathcal{C}}$ are unity. As mentioned, with a g_k -fold degenerate energy subspace $\{|E_{k,1}\rangle, \dots, |E_{k,g_k}\rangle\}$, we can generate $g_k - 1$ dark states. In this subspace, there exists one additional state, which we call the bright state, and it is given by [55]

$$|\beta_k\rangle = N\hat{P}_k|\psi_d\rangle, \quad (11)$$

where $\hat{P}_k := \sum_{m=1}^{g_k} |E_{k,m}\rangle\langle E_{k,m}|$ is the eigenspace projector. This state is not an eigenvector of the survival operator. Its mathematical property is that it is orthogonal to all the $g_k - 1$ dark states in its energy sector. This state, under repeated measurements, without conditioning the outcome, will be eventually detected with probability one; hence, it is called a bright state. In the next section, we will show how to use these bright states to construct the eigenstates of the survival operator $\hat{\mathcal{C}}$ with eigenvalues in the unit disk, i.e., $0 < |\xi| < 1$.

To recapitulate this part, we have seen that the operator $\hat{\mathcal{C}}$ has an eigenvalue zero and we have formally found the normalized left and right eigenvectors which are not parallel

$\langle \xi^L | \xi^R \rangle \neq 1$. Using the energy representation, we saw that dark states of the system are eigenvectors of the survival operator, with eigenvalue $\xi = \exp(-iE_k\tau)$. Clearly $|\xi| = 1$, so these have the maximum possible eigenvalue magnitude, since in general $|\xi| \leq 1$. In this case the left and right eigenvalues are parallel $\langle \xi^L | \xi^R \rangle = 1$. In a degenerate sector $\{|E_{k,l}\rangle\}$ of the Hilbert space, we have $g_k - 1$ such eigenvectors that are given in Eq. (8) and they all share the same eigenvalue $\exp(-iE_k\tau)$.

For example, consider a system with three distinct energy levels, the first with degeneracy 10, the second with degeneracy 5, and another with no degeneracy. Further assume for simplicity that all the energy states have finite amplitude on the detected state. Equation (8) specifies 13 orthonormal eigenstates of the survival operator, all with eigenvalues on the unit circle. These are dark states as mentioned, namely, states that cannot be detected even if we do not condition the measurements. However, if we consider the case where we choose the detected state as the energy eigenstate of the nondegenerate level, it then immediately follows from standard quantum mechanics that the remaining 15 states are all dark as they are orthogonal to the detected state. Hence, these 15 states are dark, and they are also eigenvectors of the survival operator $\hat{\mathcal{C}}$.

If the system has no degeneracy, for example, a typical random system with no symmetry in H , and if all the energy states have finite overlaps with the detected one (even small), we reach the conclusion that we have no dark states, and hence we do not have eigenstates of the survival operator with eigenvalues $|\xi| = 1$. This indicates that the dynamics of systems with disorder and those without, under the condition of repeated null measurements, can have very different properties.

There exists, of course, a third family of states, which are those with $0 < |\xi| < 1$, namely, the eigenvalues all lie inside the unit circle. There is no simple way to determine the values of ξ and find the corresponding states. However, there is an elegant method to find these eigenvalues in principle based on a classical charge theory [50], which is discussed below. With this classical theory, we will be able to gain physical insight into the largest eigenvalues of systems with no dark states, which in turn will give the long-time dynamics of the conditioned measurement process.

III. CLASSICAL CHARGE PICTURE MAPPING AND BIORTHOGONAL EIGENSTATES

As previously mentioned, the dark states are eigenfunctions of the survival operator with a special property; their eigenvalues are on the unit circle. However, the dark states are certainly not the only eigenstates of the survival operator, namely, the dark space $\mathcal{H}_D := \text{Span}(\{|\delta_{k,m}\rangle\})$ is a subspace of the full Hilbert space \mathcal{H} , so we need to search for the other eigenstates. The eigenvalues of the remaining states, which are now investigated, all fall inside the unit circle. Using the matrix determinant lemma [71], the eigenvalues of the survival operator $\hat{\mathcal{C}}$ are given by (see Appendix A)

$$\det[\xi \mathbb{1} - \hat{\mathcal{C}}] = \det[\xi \mathbb{1} - \hat{U}(\tau)] \times \langle \psi_d | [\xi \mathbb{1} - \hat{U}(\tau)]^{-1} | \psi_d \rangle \xi = 0. \quad (12)$$

We observe the following:

(i) There is a stationary point, denoted ξ_0 , located at the origin, namely $\xi_0 = 0$ [see the last term in Eq. (12)]. We have found its left and right eigenvectors in the former section.

(ii) For simplicity, let us assume all elements of the energy basis $\{|E_{k,l}\rangle\}$ have finite overlaps with $|\psi_d\rangle$. Using this energy basis, we find

$$\det[\xi \mathbb{1} - U(\tau)] = \prod_{k=0}^{w-1} (\xi - e^{-iE_k\tau})^{g_k}. \tag{13}$$

We have here a multiplication of ϖ terms $(\xi - e^{-iE_k\tau})$, where ϖ is the size of the full Hilbert space and w is the number of distinct energy levels, namely $\sum_{k=0}^{w-1} g_k = \varpi$. Only in the absence of degeneracy, $g_k = 1$, do we have $\varpi = w$. Here following Grünbaum *et al.* [50,51], we use the symbol w , as this is actually describing a certain winding number of the problem. Naively, it seems from Eq. (13) that we already have all ϖ ξ 's that satisfy Eq. (12). However, this intuition is not true because $\langle\psi_d|[\xi \mathbb{1} - \hat{U}(\tau)]^{-1}|\psi_d\rangle$ cancels part of them, as we now show.

(iii) The bright and dark space, i.e., $\{|\beta_i\rangle^{w-1}\}$ and $\{|\delta\rangle\}$, form a complete basis. Importantly, $|\psi_d\rangle$ is orthogonal to the dark states by definition. It follows that we can expand the detected state in terms of the bright subspace only:

$$|\psi_d\rangle = \sum_{k=0}^{w-1} \langle\beta_k|\psi_d\rangle |\beta_k\rangle. \tag{14}$$

The bright states $\{|\beta_k\rangle^{w-1}\}$ are also eigenstates of H and hence of $\hat{U}(\tau)$. It follows that

$$\langle\psi_d|[\xi \mathbb{1} - \hat{U}(\tau)]^{-1}|\psi_d\rangle = \sum_{k=0}^{w-1} \frac{|\langle\beta_k|\psi_d\rangle|^2}{\xi - e^{-iE_k\tau}}. \tag{15}$$

Using Eqs. (12), (13), (14), and (15), the equation for ξ 's reads as

$$\sum_{k=0}^{w-1} |\langle\beta_k|\psi_d\rangle|^2 (\xi - e^{-iE_k\tau})^{g_k-1} \prod_{i \neq k} (\xi - e^{-iE_i\tau})^{g_i} = 0. \tag{16}$$

From here we see that if the energy level E_k is degenerate, $g_k > 1$, then we find the survival operator $\hat{\mathcal{S}}$ has the eigenvalue $\xi = \exp(-iE_k\tau)$, which is $(g_k - 1)$ -fold degenerate. In contrast, if $g_k = 1$, $\xi = \exp(-iE_k\tau)$ is clearly not an eigenvalue of $\hat{\mathcal{S}}$. This coincides with what we have found in the previous section: any degenerate subspace with energy E_k has $g_k - 1$ dark states and one bright state. The $(g_k - 1)$ -fold degenerate eigenvalue of the survival operator $\xi = \exp(-iE_k\tau)$ corresponds to the $g_k - 1$ dark states found in Eq. (8). The total number of dark states is $\sum_{k=0}^{w-1} (g_k - 1) = \varpi - w$. These states have the largest possible eigenvalue magnitude $|\xi| = 1$ of $\hat{\mathcal{S}}$, hence, they will control the long-time dynamics of the conditional measurements process (see below). For disordered, interacting, or chaotic systems, where repulsion of energy levels arises, namely $g_k = 1$ for all the energy levels, we cannot find eigenvalues on the unit circle in general. In this case, $\varpi = w$ and $\sum_{k=0}^{w-1} (g_k - 1) = 0$.

(iv) The other eigenvalues $0 < |\xi_i| < 1$ are given by

$$\langle\psi_d|[\xi \mathbb{1} - \hat{U}(\tau)]^{-1}|\psi_d\rangle = 0. \tag{17}$$

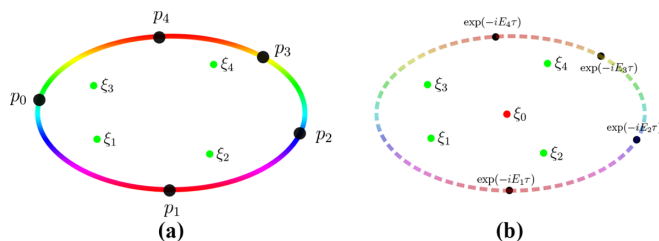


FIG. 2. Schematic depiction of the classical charge mapping [50] (a) and the eigenvalues of the survival operator $\hat{\mathcal{S}}$ (b). We plot a system with energy levels E_0, \dots, E_4 , where all the energy levels are twofold degenerate, except for E_0 which is nondegenerate. According to the charge picture, we have five charges on the unit circle, as shown on the left, with the charges being p_0, \dots, p_4 . These charges are located on $\exp(-iE_k\tau)$ from Eq. (18). All these charges are positive, and hence this gives four stationary points in the unit disk denoted ξ_1, \dots, ξ_4 in ((a). These, as explained in the text, give the nonzero eigenvalues of the survival operator inside the unit circle $0 < |\xi_i| < 1$. In (b), we plot all the eigenvalues of $\hat{\mathcal{S}}$. There are three types of eigenvalues, i.e., $|\xi| = 1, 0 < |\xi| < 1$, and $\xi_0 = 0$. The degeneracy of the energy levels leads to the dark states, which are eigenstates of $\hat{\mathcal{S}}$ with eigenvalues $\exp(-iE_k\tau)$ on the unit circle (b). The eigenvalues in the unit circle are given by the charge picture, and finally there is one eigenvalue that is at the center of the unit disk. Note that the nondegenerate energy level E_0 does not contribute a dark state.

It turns out that there are $w - 1$ ξ 's that satisfy $0 < |\xi_i| < 1$. So we see, we have $\varpi - w$ eigenvalues on the unit circle $|\xi| = 1$, $w - 1$ in the unit disk $0 < |\xi| < 1$, and one with $\xi = 0$. $(\varpi - w) + (w - 1) + 1 = \varpi$, all the eigenvalues of survival operator $\hat{\mathcal{S}}$ are found.

The question remains: How do we find the eigenvalues satisfying $0 < |\xi_i| < 1$? Here we exploit a beautiful mapping of the problem to a classical charge theory, following the work of Grünbaum *et al.* [50,72,73]. By defining $p_k = \langle\psi_d|\hat{P}_k|\psi_d\rangle = \sum_{i=1}^{g_k} |\langle E_{k,i}|\psi_d\rangle|$, together with Eqs. (11), (15), and (17), we get

$$\mathcal{F}(\xi) = \sum_{k=0}^{w-1} \frac{p_k}{\xi - e^{-iE_k\tau}} = 0. \tag{18}$$

$\mathcal{F}(\xi)$ can be considered as a two-dimensional electrostatic field created by point charges p_k at positions $e^{-iE_k\tau}$ (see Fig. 2). These charges produce a logarithm potential, namely, they can be viewed as long wires piercing the unit disk. Equation (18) defines the stationary points of this classical field. Namely, when we put a test charge into this field, the stationary points $\{\xi_i\}$ are the locations where the net force on the test charge is zero. All the $\{\xi_i\}$ are inside the unit disk ($|\xi_i| < 1$), which is rather obvious since all the charges p_k are positive.

To summarize, to find the eigenvalues according to the classical charge picture, we consider (i) w charges that are placed on the unit circle, where w is the number of distinct energy levels of H ; (ii) these charges are located at the phases $\exp(-iE_k\tau)$, where E_k are the energy levels of H ; (iii) the charges have magnitude p_k ; (iv) with these positive charges, we have $w - 1$ zeros of the force field, all inside the unit disk; (v) once we calculate these zeros, these are the eigenvalues

$0 < |\xi| < 1$ we are looking for. The charge theory is useful as it allows us to easily identify the largest eigenvalue of the survival operator in certain limits of the problem discussed below.

A. Eigenvectors of the survival operator

Now we formally find the eigenvectors of $\hat{\mathcal{S}}$ that correspond to the eigenvalues that are inside the unit circle. Here we take advantage that the dark states are already eigenstates of $\hat{\mathcal{S}}$ that correspond to eigenvalues on the unit circle. Furthermore, as mentioned, the dark and bright subspaces form a complete basis. With these two preconditions, we expand $|\xi^R\rangle$ in terms of the bright states, under the condition that the eigenvalue of $|\xi^R\rangle$ is inside the unit circle. As presented in Appendix B, we find

$$|\xi^R\rangle = N \sum_{j=0}^{w-1} \hat{R}_{i,j}^\dagger |\psi_d\rangle, \quad \hat{R}_{i,j}^\dagger = \frac{\hat{P}_j}{\xi_i - e^{-iE_j\tau}}. \quad (19)$$

Using Eq. (11), we see that the states $\{|\xi^R\rangle\}$ indeed are linear combinations of the bright states $\{|\beta_k\rangle\}$ as stated. So, $|\xi^R\rangle$ is a bright state as well, namely in the absence of conditioning, starting in this state, detection (a click yes) is eventually guaranteed. Although both $\{|\beta_k\rangle\}$ and $\{|\xi^R\rangle\}$ are bright states, the latter are eigenstates of the survival operator $\hat{\mathcal{S}}$ with corresponding eigenvalues $\{\xi_i\}$ in the unit disk, while the former are eigenstates of H and $\hat{U}(\tau)$. Note that the right eigenvectors of $\hat{\mathcal{S}}$ do not have to be orthogonal with each other, i.e., $\langle \xi_i^R | \xi_{i'}^R \rangle \neq \delta_{i,i'}$.

In Eq. (19), the $\{|\xi_i^R\rangle\}$ are presented in an energy basis, in which the evolution operator $\hat{U}(\tau)$ is diagonal. Using the identity $\sum_{j=0}^{w-1} \hat{P}_j = 1$, we have $[\xi_i \mathbb{1} - \hat{U}(\tau)]^{-1} = \sum_{j,j'=0}^{w-1} \hat{P}_j [\xi_i - e^{-iE_j\tau}]^{-1} \hat{P}_{j'}$. So

$$|\xi_i^R\rangle = N [\xi_i \mathbb{1} - \hat{U}(\tau)]^{-1} |\psi_d\rangle, \quad (20)$$

independent of any representation. The geometry of the right eigenstates is that they are all orthogonal with respect to the detection state. This is easy to see using Eq. (1), and $\langle \psi_d | (\mathbb{1} - D) = 0$.

Here we present a direct proof that Eq. (20) is indeed the right eigenvector of $\hat{\mathcal{S}}$. We start from the definition of the right eigenvectors. Using Eq. (3), we have

$$(\hat{U} - \xi_i \mathbb{1}) |\xi_i^R\rangle = |\psi_d\rangle \langle \psi_d | \hat{U} |\xi_i^R\rangle. \quad (21)$$

Inserting Eq. (20) into (21), we get

$$-|\psi_d\rangle = |\psi_d\rangle \langle \psi_d | \frac{\hat{U}}{\xi_i \mathbb{1} - \hat{U}} |\psi_d\rangle, \quad (22)$$

which leads to $-1 = \langle \psi_d | \hat{U} / (\xi_i \mathbb{1} - \hat{U}) | \psi_d \rangle$. Using $\hat{U} / (\xi_i \mathbb{1} - \hat{U}) + 1 = \xi_i \mathbb{1} / (\xi_i \mathbb{1} - \hat{U})$, we get for $\xi_i \neq 0$

$$\langle \psi_d | [\xi_i \mathbb{1} - \hat{U}]^{-1} |\psi_d\rangle = 0. \quad (23)$$

From Eq. (17), this is the equation for the eigenvalues of the survival operator $\hat{\mathcal{S}}$ that are inside the unit circle, i.e., $0 < |\xi| < 1$. Hence, Eq. (20) is correct.

Following the same procedure, the left eigenvectors of survival operator read as

$$\langle \xi_i^L | = N \sum_{j=0}^{w-1} \langle \psi_d | L_{i,j}, \quad L_{i,j} = \frac{\hat{P}_j e^{-iE_j\tau}}{\xi_i - e^{-iE_j\tau}}. \quad (24)$$

Similar to Eq. (20), we have

$$\langle \xi_i^L | = N \langle \psi_d | \hat{U}(\tau) [\xi_i \mathbb{1} - \hat{U}(\tau)]^{-1}. \quad (25)$$

The right and left eigenvectors obey the biorthogonal relation $\langle \xi_i^L | \xi_{i'}^R \rangle = N_i \delta_{i,i'}$. Here N_i is a constant which depends on how we normalize the two right and left vectors. Furthermore, the right and left eigenvectors are orthogonal to the dark states $\langle \delta_{k,j} | \xi_i^R \rangle = 0$ and $\langle \xi_i^L | \delta_{k,j} \rangle = 0$ since the dark subspace is orthogonal to the bright subspace.

B. Phase gained under repeated measurements

We now explain the physical meaning of ξ . Using Eqs. (20) and (25), if the system starts with the normalized right eigenstate $|\xi_i^R\rangle$, i.e., $|\psi_{in}\rangle = |\xi_i^R\rangle$, we have (Appendix C)

$$|\xi_i^R\rangle \xrightarrow{\hat{U}(\tau)} |\xi_i^L\rangle^* \xrightarrow{(\mathbb{1}-D)} |\xi_i^R\rangle, \quad |\xi_i^R\rangle \xrightarrow{\hat{\mathcal{S}}} |\xi_i^R\rangle, \quad (26)$$

where $*$ is the complex conjugate. We have used the fact that $|\xi_i^R\rangle$ is an eigenstate of $\hat{\mathcal{S}}$, so $\hat{\mathcal{S}} |\xi_i^R\rangle \rightarrow |\xi_i^R\rangle$. Using Eq. (2), the wave function of the system after n measurements reads as

$$|\psi_n\rangle = N_n \xi_i^n |\xi_i^R\rangle, \quad (27)$$

where N_n is a normalization constant. In this process, the operations $\hat{U}(\tau)$ and $(\mathbb{1} - D)$ send the wave function to the $|\xi_i^L\rangle^*$ and $|\xi_i^R\rangle$ n times. Importantly, we gain an unusual phase, namely,

$$|\psi_n\rangle = \exp(in\phi) |\xi_i^R\rangle = \exp(in\phi) |\psi_{in}\rangle, \quad (28)$$

where $\phi = -i \ln(\xi_i / |\xi_i|)$. This phase is not determined by the energy times evolution time, but is given by the phase of the complex eigenvalue ξ_i of the survival operator $\hat{\mathcal{S}}$. As we repeat the measurements, the system is driven periodically, and the phase accumulated is $n\phi$. We note that during a period τ , the evolution is unitary, and hence the dynamical phase, according to Aharonov and Anandan [74,75], is $E_i\tau$ as usual ($E_i = \langle \xi_i^L | H | \xi_i^R \rangle$), which clearly differs from our ϕ . This indicates that a geometric part contributes since the effect of measurement is crucial. We also note some related investigations are made in Refs. [76–79], where measurement-induced phases with unconditional weak measurements were considered.

C. Exceptional points: Example of a two-level system

In the above discussion we assumed that the system has no exceptional points. Exceptional points are cases, where for specific τ , or for certain control parameters of H , we have two (or more) eigenvalues ξ ($|\xi| < 1$) of the survival operator $\hat{\mathcal{S}}$ merging, a kind of degeneracy found for non-Hermitian physical systems [80]. In this subsection, we illustrate part of the effects with the simplest example: the two-level system, also presenting the exceptional point and its meaning. A more

general discussion about the exceptional points is presented in Sec. IX.

For a two-level system with state $|l\rangle$ (left) and $|r\rangle$ (right), the Hamiltonian reads as $H = -\gamma(|l\rangle\langle r| + |r\rangle\langle l|)$ where γ is the hopping amplitude between these two states. The energies in this system are $E_1 = -\gamma$ and $E_2 = \gamma$. We assume that we detect the particle on the left node, so $D = |l\rangle\langle l|$. In this basis the survival operator is

$$\hat{\mathcal{S}} = (\mathbb{1} - D)\hat{U}(\tau) = \begin{pmatrix} 0 & 0 \\ i \sin(\gamma\tau) & \cos(\gamma\tau) \end{pmatrix}. \quad (29)$$

We easily find the following eigenvalues and vectors of $\hat{\mathcal{S}}$:

$$\begin{aligned} \xi = 0 : & \langle \xi^L | = \langle l |, \quad | \xi^R \rangle = \cos(\gamma\tau)|l\rangle - i \sin(\gamma\tau)|r\rangle; \\ \xi = \cos(\gamma\tau) : & \langle \xi^L | = i \sin(\gamma\tau)\langle l | + \cos(\gamma\tau)\langle r |, \quad | \xi^R \rangle = |r\rangle \end{aligned} \quad (30)$$

We see from here the features discussed above, for example, for the eigenvalue $\xi = 0$ the left eigenstate is $\langle \xi^L | = \langle \psi_d |$, which in this model is $\langle \xi^L | = \langle l |$. Further

$$\hat{U}(\tau) = \begin{pmatrix} \cos(\gamma\tau) & i \sin(\gamma\tau) \\ i \sin(\gamma\tau) & \cos(\gamma\tau) \end{pmatrix}, \quad (31)$$

and hence for the second eigenvalue $\xi = \cos(\gamma\tau)$ and vector $| \xi^R \rangle = |r\rangle$, we have $\hat{U}(\tau)| \xi^R \rangle = i \sin(\gamma\tau)|l\rangle + \cos(\gamma\tau)|r\rangle = | \xi^L \rangle^*$. Then the conditional measurement $(\mathbb{1} - D)$ wipes out the amplitude on $|l\rangle$, which leads to $(\mathbb{1} - D)| \xi^L \rangle^* \rightarrow |r\rangle = | \xi^R \rangle$. This is an illustration of Eq. (26).

According to our formalism, in the large- n limit the state of the system is determined by the eigenvector corresponding to the eigenvalue closest to the unit circle, i.e., $\max(0, |\cos(\gamma\tau)|)$ which, unless $|\cos(\gamma\tau)| = 0$, means $\lim_{n \rightarrow \infty} |\psi_n\rangle = |r\rangle$. This is easy to understand, as after the null measurements, the system cannot be on $|l\rangle$. Since there are only two states, we find the system after the n th measurement on $|r\rangle$. This holds true for any n .

The exceptional point is found when $\cos(\gamma\tau) = 0$, and for this case $\hat{\mathcal{S}}$ cannot be diagonalized at all. Three features are found: (a) in this limit, Eq. (30) gives $\langle \xi^L | \xi^R \rangle = 0$; (b) the two eigenvalues coalesce on zero, i.e., $\xi = 0$; finally (c) the two pairs of vectors, both L and R , in Eq. (30) become parallel (in our representation, aside from an i they are identical). Thus, at the exceptional sampling time $\tau = (\pi/2 + k\pi)/\gamma$, where k is an integer, we have only one eigenvector instead of the familiar two. This means that both the eigenvalues and the eigenvectors coalesce, which implies an exceptional point. Mathematically, when $\cos(\gamma\tau) = 0$, the survival operator now reads as

$$\hat{\mathcal{S}} = (\mathbb{1} - D)\hat{U}(\tau) = \begin{pmatrix} 0 & 0 \\ i & 0 \end{pmatrix} \quad (32)$$

and then the eigenvalues are clearly zero, and we have only one eigenvector solution instead of two.

How can we search for these exceptional points without solving the problem exactly? We claim that we can use the classical charge picture, which is very useful in determining the exceptional points in general. Let us present it for the two-level system so that the reader can get familiarized with the basic ideas. We situate the classical charges on the unit

circle. The location of the pair of charges is on the phases $\exp(-iE_1\tau) = \exp(i\gamma\tau)$ and $\exp(-iE_2\tau) = \exp(-i\gamma\tau)$. The magnitudes of the charges in our example are identical and positive. Then we search for the stable point, namely, the point in space where the classical force field of the charges vanishes. This is clearly on the midpoint connecting the two charges. From basic geometry, we realize that this classical stable point is found in this example on $\xi = \cos(\gamma\tau)$ in the complex plane. Especially, if we choose τ such that these charges are on the north and south poles, the stable point is on the origin, in agreement with Eq. (30). This describes the coalescence at the stationary point. Dynamically, we imagine the eigenvalue $\cos(\gamma\tau)$ moving to the origin where it fuses with the ever-present eigenvalue $\xi = 0$ there. By moving, we mean that we think of the process as we tune $\gamma\tau$. We may control this fusing process with the rearrangement of the charges on the unit circle, i.e., moving them to the south and north poles. The mapping of the problem to a classical charge theory allows for an intuitive understanding when exceptional points emerge, in generality, and shows how this is related to the symmetry of the problem.

For the two-level system, what is the physical meaning of the exceptional point? When the system is tuned to this point, and we attempt to follow the null measurements, we encounter a problem. After the first measurement, we get a null result, as this is the condition imposed by the rules of the model. But now, after the first measurement, the system is in state $|r\rangle$ (since we conditioned the measurements to give a no when we detect on $|l\rangle$). However, when $\cos(\gamma\tau) = 0$, we will find the state of the system just before the second measurement in the state $|l\rangle$. We then perform the second measurement and find the system in the detected state $|l\rangle$ with probability one. It follows that we tried to impose the sequence of null measurements. However, at the exceptional points, this is impossible since we always get a yes in the second measurement. This feature is generic, and found below in systems whose complexity exceeds that of a two-level example.

IV. STATE FUNCTION UNDER CONDITIONED MEASUREMENTS

A useful identity which holds for non-Hermitian operators and is not limited to our case reads as [81–83]

$$\sum_{\xi} \frac{| \xi^R \rangle \langle \xi^L |}{\langle \xi^L | \xi^R \rangle} = 1. \quad (33)$$

This formula is valid provided that we do not have exceptional points in the system. The summation is over all the states in the system, denoted by the sum over the index ξ . It follows from Eq. (33) that a generic initial condition can be expanded like

$$|\psi_{in}\rangle = \sum_{\xi} \frac{\langle \xi^L | \psi_{in} \rangle | \xi^R \rangle}{\langle \xi^L | \xi^R \rangle}. \quad (34)$$

For the case under study, we split the sum into three parts, those with eigenvalues on the unit circle $|\xi| = 1$, $\xi = 0$, and

all the rest:

$$|\psi_{in}\rangle = \underbrace{\frac{\langle\psi_d|\psi_{in}\rangle}{\langle\psi_d|U^{-1}|\psi_d\rangle}U^{-1}|\psi_d\rangle}_{\xi=0} + \sum_{0<|\xi|<1} \frac{\langle\xi^L|\psi_{in}\rangle}{\langle\xi^L|\xi^R\rangle}|\xi^R\rangle + \sum_{\delta,|\xi|=1} \langle\delta|\psi_{in}\rangle|\delta\rangle. \tag{35}$$

The first term, proportional to $U(\tau)^{-1}|\psi_d\rangle$, has a clear physical meaning since after the first time interval τ , the unitary

evolution yields $UU^{-1}|\psi_d\rangle = |\psi_d\rangle$. The first detection is modeled with the projector $(\mathbb{1} - D)$ and hence this first term is wiped out by the first measurement. As mentioned, if $|\psi_{in}\rangle = \hat{U}^{-1}|\psi_d\rangle$, we cannot get the conditional measurements, namely, for this initial condition, we record a yes at the first measurement attempt, so it is important for our discussion that the second and third terms are nonzero. In Eq. (35), we assume $\langle\psi_d|U^{-1}|\psi_d\rangle \neq 0$ and $\langle\xi^L|\xi^R\rangle \neq 0$, otherwise we get an exceptional point. Using Eqs. (2), (3), and (35), the wave function after $n \geq 1$ measurements reads as

$$|\psi_n\rangle = N \left\{ \sum_{0<|\xi|<1} \xi^n \frac{\langle\xi^L|\psi_{in}\rangle}{\langle\xi^L|\xi^R\rangle} |\xi^R\rangle + \sum_{\delta,|\xi|=1} \exp(-iE_\delta n\tau) \langle\delta|\psi_{in}\rangle |\delta\rangle \right\}, \tag{36}$$

and N is the normalization. In the next section we use this equation to explore the large- n limit of the system. Here we see that in general the state of the wave function is composed of dark states $|\delta\rangle$ with eigenvalues $\exp(-iE_\delta\tau)$ and bright states $|\xi^R\rangle$ with eigenvalues $0 < |\xi| < 1$. The effect of the state with eigenvalue $\xi = 0$ is washed out after the first measurement.

We now consider the mean energy of the system. Even though the particle is not detected, there must be an exchange of energy between the system and the detector, hence, the energy of the particle is not constant. Initially, the expectation of the energy of the system is $\mathcal{E}_0 = \langle\psi_{in}|H|\psi_{in}\rangle$. Due to the measurements, the average energy of the system after the n th measurement is $\langle\mathcal{E}_n\rangle = \langle\psi_n|H|\psi_n\rangle$. Using Eq. (36), we have

$$\langle\mathcal{E}_n\rangle = \frac{\sum_{0<|\xi, \xi'|<1} a_\xi a_{\xi'}^* \xi^n (\xi'^*)^n \langle\xi^R|H|\xi^R\rangle + \sum_{\delta,|\xi|=1} |\langle\delta|\psi_{in}\rangle|^2 E_\delta}{\sum_{0<|\xi, \xi'|<1} a_\xi a_{\xi'}^* \xi^n (\xi'^*)^n \langle\xi^R|\xi^R\rangle + \sum_{\delta,|\xi|=1} |\langle\delta|\psi_{in}\rangle|^2}, \tag{37}$$

where $a_\xi = \langle\xi^L|\psi_{in}\rangle/\langle\xi^L|\xi^R\rangle$, and $\langle\tilde{\xi}^R|H|\xi^R\rangle = \sum_{k=0}^{w-1} p_k E_k / [(\tilde{\xi} - e^{iE_k\tau})(\xi - e^{-iE_k\tau})]$. If initially the system is prepared in a linear combination of dark states, then clearly the energy is a constant of motion, but otherwise it is not. In particular, if we have no dark states in our system, namely, no symmetry and hence no degeneracy, the measurements never conserve energy. Note that in this case the mean energy can saturate for large n , or exhibit dynamical oscillations, which are explored below.

V. FIXED STATE AND QUANTUM DYNAMICS

From Eq. (36), in the large- n limit, we reach several general conclusions:

(a) If the dark subspace is not empty, namely, if we have some degenerate energy levels (implying some symmetry in the system) or if one of the stationary states of H is orthogonal to $|\psi_d\rangle$, the second term in Eq. (36) dominates the large- n limit provided that the initial condition $|\psi_{in}\rangle$ has some overlap with the dark states. This means that the long-time dynamics is determined by the phases $\exp(-iE_\delta n\tau)$. Compared to unitary dynamics, where all the energy levels contribute, the effect of measurement is therefore to remove the nondegenerate energy levels from the long-time dynamics. The wave function then reads as

$$|\psi_f\rangle = \lim_{n \rightarrow \infty} |\psi_n\rangle \sim N \sum_{\delta,|\xi|=1} e^{-iE_\delta n\tau} \langle\delta|\psi_{in}\rangle |\delta\rangle. \tag{38}$$

(b) In the case when the dark subspace is empty, as typically found for systems without special symmetries, we find two types of behaviors. We first need to determine the maxi-

um of the set $\{|\xi_i|\}$ and recall that these absolute values are all less than unity. Then, note the following:

(b1) If the maximum is unique, the system in the long-time limit goes to a specific state. There is no dynamics in this limit as only one term dominates. This is similar to a fixed point. We denote this unique largest eigenvalue of survival operator $\tilde{\mathcal{C}}$ as ξ_f . Using Eq. (36), we have

$$|\psi_f\rangle \sim N \xi_f^n |\xi_f^R\rangle = e^{in\phi_f} |\xi_f^R\rangle, \tag{39}$$

where $\phi_f = -i \ln(\xi_f/|\xi_f|)$. The system ends up with the state $|\xi_f^R\rangle$ and attains a global phase $n\phi_f$. In Eq. (28), the phase ϕ_i of the system is determined by the initial state, while here the phase ϕ_f is determined by the maximum of the set $\{|\xi_i|\}$. Furthermore, for a generic initial state, at the first stages of the processes (n is not large) many phases $\phi_i = -i \ln(\xi_i/|\xi_i|)$ contribute [see Eq. (36)]. As the component $|\xi_f^R\rangle$ gradually wins the game, the corresponding phase becomes the only term that dominates (n is large). Each application of $\tilde{\mathcal{C}}$ rotates the phase of the system by ϕ_f .

(b2) If the maximum of the set $\{|\xi_i|\}$ is shared by several eigenvalues of the survival operator $\tilde{\mathcal{C}}$, all with the same absolute value but with different phases, then these eigenvalues will control the large- n limit of Eq. (36). In this case, the wave function, for large n , will exhibit nontrivial dynamic. The system not only gains a global phase like the above case (b1), but also exhibits interference due to the relative phases of these eigenvalues.

As an example, consider two eigenvalues $|\xi_1| = |\xi_2| > |\xi_i|$ ($i \neq 1, 2$) and $|\xi_1| = |\xi_2| < 1$, we denote $\xi_1 = r e^{i\phi_1}$ and $\xi_2 = r e^{i\phi_2}$, where $r = |\xi_1| = |\xi_2|$, $\phi_1 = -i \ln(\xi_1/|\xi_1|)$, and $\phi_2 = -i \ln(\xi_2/|\xi_2|)$. Using Eq. (36), the terms with

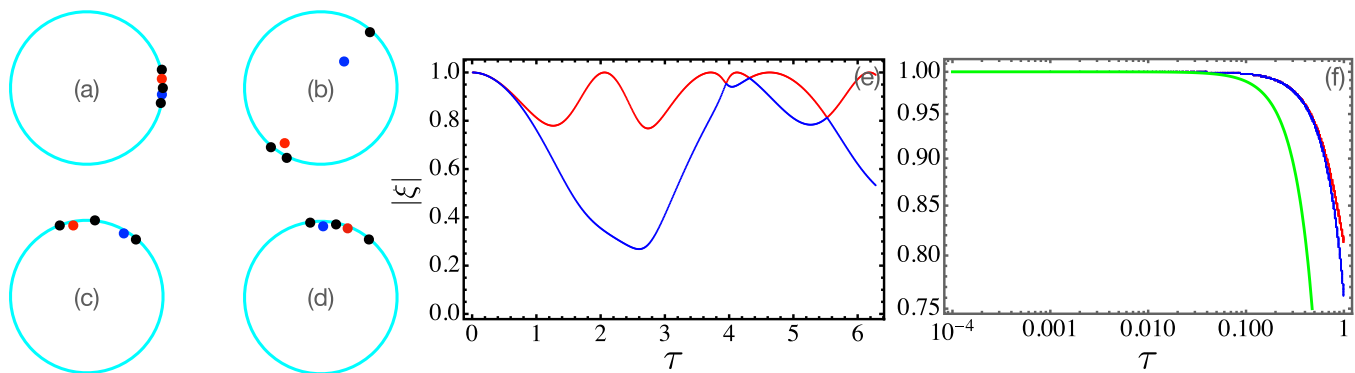


FIG. 3. The absolute values of the eigenvalues ξ_1 (red) and ξ_2 (blue) versus τ are presented in (e) and (f). (a)–(d) Charge configurations for $\tau = 0.1$ (a), $\tau = 2$ (b), $\tau = 4.31697$ (c), and $\tau = 4$ (d). The black points are charges located on the unit disk. The red and blue points are stationary points (eigenvalues of $\hat{\mathcal{C}}$) ξ_1 and ξ_2 . In this simple model, we have two eigenvalues ξ_1 and ξ_2 that are inside the unit circle. The eigenvalues with larger magnitude determine the final state of the system in the large- n limit. When the curves in (e) cross, namely $|\xi_1| = |\xi_2|$, we find persistent quantum oscillations, for example for the energy. In the Zeno limit (a), $\tau \rightarrow 0$, both eigenvalues approach unity. A comparison with the lower bound (42) (green line) is presented in (f). Note the usefulness of the charge picture. For example in (a), since τ is small, all the charges, i.e., black points on the unit disk, are closely situated, and it follows from basic electrostatics that also the eigenvalues (red and blue points) are both close to unity. This is shown clearly in subplot (e) in the small- τ limit.

eigenvalues ξ_i ($i \neq 1, 2$) decay away, and we are left with $|\psi_f\rangle = |\psi_n\rangle \sim N(a_1 r^n e^{in\phi_1} |\xi_1^R\rangle + a_2 r^n e^{in\phi_2} |\xi_2^R\rangle) = N r^n (a_1 e^{in\phi_1} |\xi_1^R\rangle + a_2 e^{in\phi_2} |\xi_2^R\rangle)$ (as a reminder, a_i is the overlap with the initial state). r^n can be absorbed by the normalization. In the end, we have

$$|\psi_f\rangle \sim N e^{in\frac{\phi_1+\phi_2}{2}} (a_1 e^{in\frac{\phi_1-\phi_2}{2}} |\xi_1^R\rangle + a_2 e^{in\frac{\phi_2-\phi_1}{2}} |\xi_2^R\rangle). \quad (40)$$

Comparing with Eq. (39), where there are two ξ 's that dominate the large- n evolution, the system not only gains a global phase $(\phi_1 + \phi_2)n/2$ in the measurement process, but also exhibits an oscillation that is controlled by the relative phase $(\phi_1 - \phi_2)n/2$ of ξ_1 and ξ_2 . We can tune this relative phase by changing the sampling time interval τ (see Sec. VIII). Mean observables, like the energy, may thus exhibit periodic controllable oscillations (see our examples below). In this process, the system is steered periodically by the repeated measurements, and we call this interesting phenomena quantum dynamics induced by the measurements.

VI. THREE-LEVEL SYSTEM, V-SHAPED SYSTEM

The two-level system example, treated in Sec. III C, is obviously a very special case, and misses a lot of the different dynamical regimes. We now consider a three-level system, with no dark states. According to the theory developed, we will have two eigenvalues ξ_1 and ξ_2 , aside from $\xi_0 = 0$, in the unit disk and the long-time limit of the system will be determined by the eigenvalue which is larger in magnitude in absolute value sense. When we vary, say τ , we can find different cases. When $|\xi_1| = |\xi_2| \neq 0$, the relative phase of these eigenvalues will play a special role, namely, we then expect oscillatory behavior to persist forever. This is investigated here with an example using the charge picture.

We consider a three-level system with the Hamiltonian

$$H = -\gamma(|0\rangle\langle 1| + |1\rangle\langle 0| + |1\rangle\langle 2| + |2\rangle\langle 1| + |0\rangle\langle 0|). \quad (41)$$

Note that we have added an onsite energy $-\gamma$ on the node labeled $|0\rangle$. The spectrum of H is given by $E_i^3 - E_i^2 - 2E_i + 1 = 0$, where we have set $\gamma = 1$. We then find $E_0 \simeq -1.25$, $E_1 \simeq 0.445$, and $E_2 \simeq 1.80$. We prepare the system initially in state $|\psi_{\text{in}}\rangle = |2\rangle$ and we perform null measurements, every τ units of time, on the detection state $|\psi_d\rangle = |0\rangle$. Using Eq. (18), there are three charges: $p_0 \simeq 0.108$, $p_1 \simeq 0.349$, and $p_2 \simeq 0.543$, located at $e^{-iE_0\tau}$, $e^{-iE_1\tau}$, and $e^{-iE_2\tau}$ (see Fig. 3 left panels). This forms our charge picture with two stationary points ξ_1 and ξ_2 inside the unit circle. Since the energy spectrum is nondegenerate, there are no dark states in the system. As demonstrated in Fig. 3, varying τ we get different charge configurations that yield different behaviors for the measurement process.

In Fig. 4, we show the energy of the system versus n for four choices of τ . Notice the different scales of n in these plots. For small τ , we find Zeno dynamics, the system is lingering in one state for very long time, but eventually switches to a state that is stable in time. The transition is seen roughly at $n = 10^5$ [see Fig. 4(a)]. In contrast, in Fig. 4(b), when $\tau = 2$, we find a steady state after roughly five measurements. This corresponds to a case where the eigenvalues ξ_1 and ξ_2 are separated, while in the Zeno case $|\xi_1| \simeq |\xi_2| \simeq 1$. The energy levels E_0 and E_2 are now nearly quasidegenerate. We get the Floquet dark state, whose energy is approximately -0.75 . We also see oscillatory behavior for the special choice of $\tau = 4.31697$ in Fig. 4(c) or when working close to this value, where the oscillations decay away eventually, Fig. 4(d). To gain insights on these behaviors we go back to the charge picture in Fig. 3.

In Fig. 3, we plot the absolute values of eigenvalues ξ_1 and ξ_2 and the corresponding charge configurations for $\tau = 0.1, 2, 4.31697, 4$. In the Zeno regime, i.e., $\tau \rightarrow 0$, all the three charges merge [see Fig. 3(a)]. Since the charges are closely situated, it is obvious from electrostatics that the stationary points are all coalescing in the vicinity of the charges but in the unit disk. This is because all the charges are positive. The eigenvalues of $\hat{\mathcal{C}}$ are $|\xi_1| \simeq |\xi_2| \simeq 1$. Hence, the system

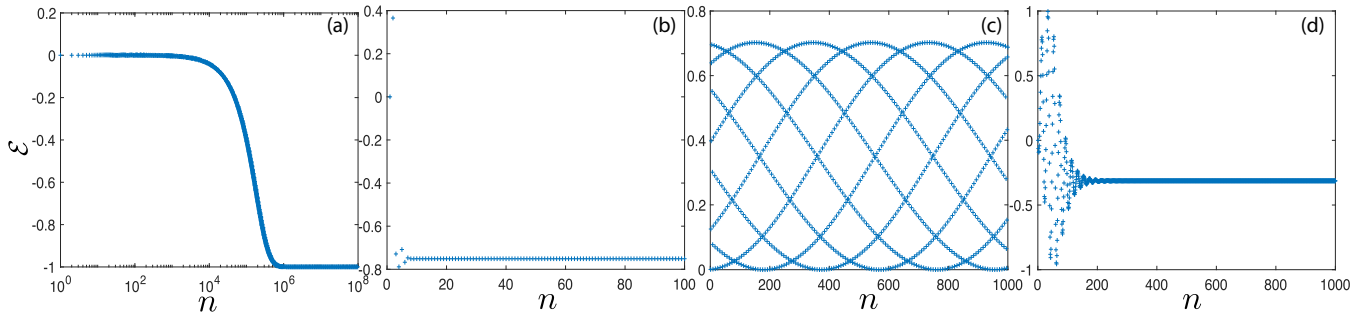


FIG. 4. The expected energy of the three-level system versus the measurements step n for $\tau = 0.1$ (a), $\tau = 2$ (b), $\tau = 4.31697$ (c), and $\tau = 4$ (d). In (a), we have $\xi_1 \sim \xi_2 \sim 1$ and $|\xi_1| > |\xi_2|$, the number of steps it takes to reach the state $|\xi_1^R\rangle$ is very large. As a comparison, in (b), $|\xi_1| \sim 1$ and $|\xi_2| \sim 0.4$, and the transition to state $|\xi_1^R\rangle$ is very fast. In (c), we have $|\xi_1| = |\xi_2|$. Hence, the energy oscillates due to the competition between the two states. (d) Close to the oscillation point but not exactly on it, so the amplitude of oscillation decays to zero.

reaches the final state slowly since clearly both $|\xi_1|^n$ and $|\xi_2|^n$ decay slowly. This behavior is generic to the Zeno limit and it will be investigated in generality in Sec. VIII. A general feature of the eigenvalues is found to be

$$|\xi_i| \geq \cos(\Delta E \tau / 2) \quad (42)$$

for small τ , where ΔE is the difference between the maximum of the energy E_{\max} and the minimum E_{\min} [50]. In our case $\Delta E \simeq 3.05$. We see, with this lower bound, that as $\tau \rightarrow 0$ all the eigenvalues of the survival operator approach unity (and hence one cannot simply neglect one compared to the other, unless n is really large). In Fig. 3(f) we plot this bound for demonstration.

In Fig. 3(b), i.e., $\tau = 2$, we have two charges that are near merging [50]. This means that the phases satisfy $\exp(-iE_0\tau) \simeq \exp(-iE_2\tau)$. From basic electrostatics, if we have two nearby charges we expect a stationary point in their vicinity, where the forces are balanced. Thus, once again we see that the charge picture can be used to rationalize our finding, and more importantly in Sec. VIII, we will present a more general theory based on it. This leads to $|\xi_1| \simeq 1$, while $|\xi_2| \simeq 0.4$. The system reaches the final state very quickly since $|\xi_1| \gg |\xi_2|$. In Fig. 3(c), $\tau = 4.31697$, $|\xi_1| = |\xi_2|$, which leads to the oscillation in Fig. 4(c) predicted in Eq. (40).

A. Artificial driven atom with V-shaped energy structure

We now consider an artificial atom system with the famous V-shaped energy level structure that allows for shelving [30] (see Fig. 5). The system's states are $|G\rangle$ (ground state) and $|D\rangle$ and $|B\rangle$. Inspired by the experiment in Ref. [32], we will investigate the case where transition amplitudes from $|G\rangle$ to $|D\rangle$ and $|G\rangle$ to $|B\rangle$ vary considerably. The system starts in the ground state, and then conditional null measurements are made in state $|B\rangle$. The question is where will we find the particle, when n is large? It turns out that the particle is shelved in state $|D\rangle$ and the amplitude of finding the particle in the ground state diminishes with n . In some sense the fact that we gain knowledge from measurements that the system is not in $|B\rangle$ implies that it cannot be found in $|G\rangle$ also since $|G\rangle$ is loosely speaking the doorway to $|B\rangle$. Thus, the energy of the system is going to increase from the energy of the ground state to the energy of state $|B\rangle$. We now investigate this scenario in

more detail. The Hamiltonian H reads as

$$H = E_D|D\rangle\langle D| + E_B|B\rangle\langle B| + E_G|G\rangle\langle G| + \gamma_1(|G\rangle\langle D| + |D\rangle\langle G|) + \gamma_2(|G\rangle\langle B| + |B\rangle\langle G|). \quad (43)$$

We first find the eigenenergies and eigenvectors of H using the basis $\{|D\rangle, |G\rangle, |B\rangle\}$. To simplify the calculations, we set $E_G = 0$, $E_D = 3$, $E_B = 5$, $\gamma_2 = 1$. We keep γ_1 as a free parameter, and we will consider the limit when it approaches zero. Then the eigenvalues E_i of H are given by $E_i^3 - 8E_i^2 + (14 - \gamma_1^2)E_i + 3 + 5\gamma_1^2 = 0$. When $\gamma_1 \rightarrow 0$, we have $(-3 + E_i)(-1 - 5E_i + E_i^2) \simeq 0$, which leads to $E_0 \simeq -0.2$, $E_1 \simeq 3$, and $E_2 \simeq 5.2$. The eigenstates of H are $|E_i\rangle = N\{(-1 - 5E_i + E_i^2)/\gamma_1, E_i - 5, 1\}^T$, where N is the normalization. As $\gamma_1 \rightarrow 0$, $|E_1\rangle \simeq |D\rangle$, a result we will use later.

We then choose $\gamma_1 = 0.01$. By the definition of charges, we have $p_0 = |\langle B|E_0\rangle|^2 \simeq 0.03576$, $p_1 = |\langle B|E_1\rangle|^2 \simeq 2.040 \times 10^{-6}$, $p_2 = |\langle B|E_2\rangle|^2 \simeq 0.9642$. So $p_2 \gg p_0 \gg p_1$, the charges p_0 and p_1 are much weaker than p_2 . In the electrostatic language, we have two weak charges and, as a result, the stationary points ξ_1 and ξ_2 will approach these weak charges separately. With simple numerical calculations, we find the eigenvalues of \hat{S} are $\xi_1 \simeq 0.0707 + 0.9975i$, $\xi_2 = 0.9292 + 0.0742i$, so $|\xi_1| \simeq |\xi_2| \simeq 1$, and $|\xi_1| > |\xi_2|$.

We see that we have a very weak charge p_1 in the system. In this case we expect and indeed find an eigenvalue of the survival operator that is very close to charge, but inside the unit circle, and it is ξ_1 . This can be understood using basic electrostatics, namely, for three positive charges on the unit circle, we expect to find a stationary point close to the weak

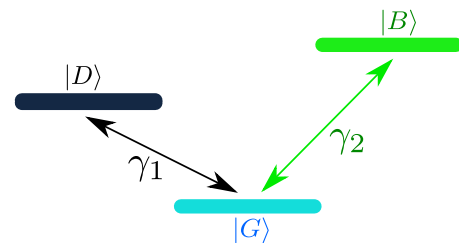


FIG. 5. Three-level V-shaped system. We initially prepare the system in the ground state $|G\rangle$. The matrix element of H describing jumping between $|G\rangle$ and $|D\rangle$ ($|B\rangle$) is γ_1 (γ_2), where $\gamma_2 \gg \gamma_1$. The detection state is the state $|B\rangle$.

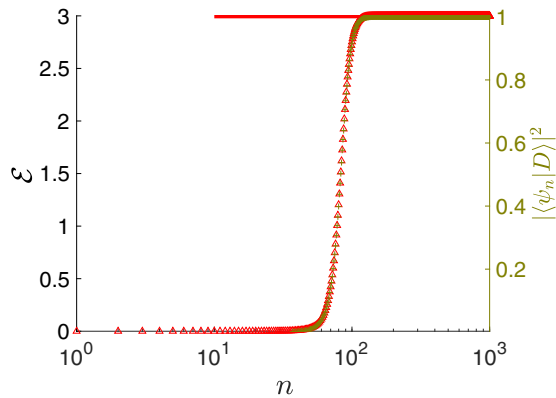


FIG. 6. From simulations, we plot the mean energy (red triangles) of the V-shaped system and the probability to be in state $|D\rangle$ (green crosses) versus n . Here we choose $\gamma_1 = 0.01$, $\gamma_2 = 1$, and $\tau = 0.5$. The red line is the theoretical prediction of the mean energy for the large- n limit from Eq. (44). The null measurements shelve the system in state $|D\rangle$.

charge, with the remaining charges balancing the force (similarly, the stationary point between Earth and Moon is closer to the Moon). We will show this in more generality in Sec. VIII, using perturbation theory, but for now we point out that to leading order we expect that the corresponding eigenstate, namely $|E_1\rangle$, is selected as the stationary state of the system. So, for a quantum particle initially in the ground state $|G\rangle$, using Eq. (49), we have for large n

$$|\psi_f\rangle \simeq e^{in\phi} |\xi_1\rangle \simeq e^{-inE_1\tau} |E_1\rangle \simeq e^{-inE_1\tau} |D\rangle. \quad (44)$$

Second, because we have two weak charges, i.e., both p_0 and p_1 are weak compared to p_2 , that leads to $|\xi_1| \simeq |\xi_2|$ as mentioned. Therefore, for not too large n , and from Eq. (36), both the eigenvalues contribute, and the transition to the final state (44) is slow. Only at a certain critical large number of measurements do we observe a transition.

As shown in Fig. 6, the expected energy of the monitored system exhibits a transition from the zero energy of the ground state $|G\rangle$ to the energy of state $|D\rangle$, which is 3. This transition is found at $n \simeq 50$, which is related to the relative magnitude of $|\xi_1|$ and $|\xi_2|$ since in this example both are close to unity as mentioned. We also plot the probability of being in state $|D\rangle$ which exhibits a transition from zero to unity similar to that seen in the expected energy.

As already mentioned in the Introduction, we have been inspired by the experiment of Mineev *et al.* [32]. There the steering by conditional measurements was used to control and reverse the quantum jump in mid-flight. This, in turn, is based on concepts of quantum trajectories, well investigated in quantum optics. There the emission events, or more generally quantum jumps, are inherent to the dynamics of the system, for example, a fluorescence process. In our approach, which is different from the experiment, we impose the jumps and the conditional steering by repeated projective measurements, where the condition is a null measurement (i.e., nondetection). We believe that due to the advances in single-particle manipulation, the proposed method will be useful both in the steering of single-particle systems, as shown here, but also for their control. For example, in the quantum search problem, the goal

of the field is to speed up the search, which in turn is presented as the time it takes for a quantum walker to reach the target state. Then, if we detect many events of failed measurements (like those analyzed here), we may wish to resort to control. By that, we mean that after observing many failed detections, the system in the search process is pushed toward a dark state. These dark states, in systems with built-in symmetry, are stable. This means that after the target is not detected for a while, it will be of benefit to add control, for instance, to restart the search process or add an external perturbation. This approach and its effect on the quantum search process will be investigated in more detail in the future.

Remark. The state $|D\rangle$ in this section is traditionally called dark, indeed this term is obviously very physical. In the context of this work, and based on our definition of the dark state $|\delta\rangle$, note that state $|D\rangle$ is only nearly dark. We defined dark states as such that starting in those states the system is never detected, while here a system initially starting in the state $|D\rangle$ can be detected, at least in principle (without conditioning the measurements, of course). The meaning of nearly dark is related to the set of parameters like γ_1 we and others use in these problems. The meaning of a nearly dark state is explored below in perturbation theory in full generality using the so-called weak charge theory (see Sec. VIII A).

VII. GLUED BINARY TREE

As another application of our general theory, we consider the glued binary tree [84,85]. Glued trees were investigated previously as they provide exponential speedup for quantum search algorithms [86,87], and this was observed in a recent experiment [88]. In contrast, we consider the effect of null measurements on this popular model.

The glued tree is a symmetric system and hence the energy spectrum is degenerate. For an initial state composed of degenerate and nondegenerate energy levels of H , we show that the null measurements drive the system into the degenerate subspace (dark states), while the nondegenerate component becomes irrelevant in the long-time limit. Hence, the measurements select the final state of the system, which acts like a “selection rule.” For instance, consider an initial state $|\psi_{in}\rangle = (|E_0\rangle + |E_1\rangle)/\sqrt{2}$, where $|E_0\rangle$ is a nondegenerate energy level of the glued tree and $|E_1\rangle$ is degenerate. Under the action of null measurements, the nondegenerate $|E_0\rangle$ component is wiped out and the final state of the system is $|\psi_f\rangle \sim |E_1\rangle$.

We also show that by periodic null measurements on node $|7, 1\rangle$ (see Fig. 7), the system can be driven to an equilibrium-steady state, where the mean energy of the system is a constant. More interesting scenarios are found when we tune the sampling time τ . We show that the local action (null measurements) on the node $|7, 1\rangle$ can drive the whole system into an oscillation mode. As shown in Figs. 9 and 12, the mean energy of the system periodically oscillates in time and such an oscillation is easy to tune with the parameter τ .

A. Eigenstates and eigenenergies

First, let us define a sequence of graphs G_d . G_d consists of two balanced binary trees [84]. The total number of vertices in G_d is $2^{d+1} + 2^d - 2$. In Fig. 7 we present the G_3 tree,

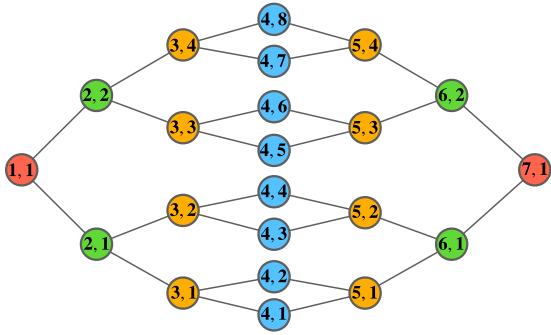


FIG. 7. Glued binary tree graph G_3 . The detector is set on the state $|1, 1\rangle$. We consider different initial states.

which will serve as our example. This graph describes the Hamiltonian of the system, namely, the nodes are the states and the links represent the hopping amplitudes between states. All transitions are identical, so that the Hamiltonian is given by the adjacency matrix of the graph.

The eigenenergies and eigenstates of this model were obtained in Refs. [84,85]. Here we briefly recap the solution of the stationary Schrödinger equation. We consider a labeling along the “columns” and “rows” of the form (j, s) (see Fig. 7), where j goes from 0 to $2d$ indicates the distance from the left root to right root along the graph, and s goes from 0 to $N_{d,j} - 1$ is the location within a given column. $N_{d,j}$ is the number of sites in a given column j , and it is given by $N_{d,j} = 2^j$ for $j \leq d$, and $N_{d,j} = 2^{2d-j}$ for $j > d$. Then, the eigenstates of H are [85]

$$|E_{k,d-v,\alpha}\rangle = \frac{1}{\sqrt{d-v+1}} \sum_{j=0}^{2(d-v)} \sin \left[\frac{k(j+1)\pi}{2(d-v+1)} \right] |\text{scol } j; \alpha, v\rangle \quad (45)$$

with

$$|\text{scol } j; \alpha, v\rangle = \sum_{s=2\alpha N_{j,d-v}}^{(2\alpha+1)N_{j,d-v}-1} \frac{|j+v, s\rangle - |j+v, s+N_{j,d-v}\rangle}{\sqrt{2N_{j,d-v}}}$$

in which $|j, s\rangle$ denote the Hilbert space vector associated with vertex (j, s) ; and $v = 0, \dots, d$; and $k = 1, \dots, 2(d-v) + 1$. In $|\text{scol } j; \alpha, v\rangle$, $j = 0, \dots, 2(d-v)$ and $\alpha = 0, \dots, 2^{v-1} - 1$. α is an integer, so when $d = 0$, $\alpha = 0$. The corresponding eigenvalues are given by [85]

$$E_{k,d-v} = -2\sqrt{2} \cos \left(\frac{k\pi}{2(d-v+1)} \right). \quad (46)$$

TABLE I. The energy spectrum of the G_3 tree. The detection state is $|\psi_d\rangle = |1, 1\rangle$. The number of states with zero and nonzero overlap with the detection state $|\psi_d\rangle$ is listed in the last two lines.

	E_0	E_1	E_2	E_3	E_4	E_5	E_6	E_7	E_8	E_9	E_{10}
Energy	$-2\sqrt{2} \cos(\pi/8)$	$-\sqrt{6}$	-2	$-\sqrt{2}$	$-2\sqrt{2} \sin(\pi/8)$	0	$-E_4$	$-E_3$	$-E_2$	$-E_1$	$-E_0$
Degeneracy	1	1	3	1	1	8	1	1	3	1	1
$\langle \psi_d E_{k,i} \rangle = 0$	0	1	0	1	0	5	0	1	0	1	0
$\langle \psi_d E_{k,i} \rangle \neq 0$	1	0	3	0	1	3	1	0	3	0	1

B. Null measurements

To present the quantum dynamics via measurements, we treat a specific model. We choose the G_3 tree as shown in Fig. 7, which consists of 22 nodes. So $d = 3$. We use Eq. (46) and for simplicity we label the energy levels according to $E_0 < E_1 < E_2 \dots < E_{10}$ (see Table I). The energy level $E_5 = 0$ is eightfold degenerate and $E_2 = 2$ and $E_7 = -2$ are threefold degenerate. Other states are not degenerate. The detection state is $|\psi_d\rangle = |1, 1\rangle$ (see Fig. 7), the eigenstates $|E_1\rangle, |E_3\rangle, |E_7\rangle, |E_9\rangle$, and $|E_{5,i}\rangle$, where $i = 4, 5, 6, 7, 8$, have no overlaps with the detected state $|\psi_d\rangle$, they are dark states by definition. Then we are left with three energy levels that are threefold degenerate, i.e., $E_2 = 2, E_7 = -2$, and $E_5 = 0$. Using Eq. (8), we construct from each degenerate energy subspace two dark states. For instance, the dark states on energy level E_2 are $|\delta_{2,1}\rangle = \sqrt{1/6}|E_{2,1}\rangle - \sqrt{5/6}|E_{2,2}\rangle$ and $|\delta_{2,2}\rangle = 1/\sqrt{6}|E_{2,1}\rangle + 1/\sqrt{30}|E_{2,2}\rangle - 2/\sqrt{5}|E_{2,3}\rangle$. Following the same procedure, we can also construct the dark states $|\delta_{5,1}\rangle, |\delta_{5,2}\rangle, |\delta_{8,1}\rangle$, and $|\delta_{8,2}\rangle$ using Eq. (8), giving us all 15 dark states in the system.

1. Quantum dynamics driven by measurements

Now, based on the charge picture approach, we show different quantum dynamics driven by repeated measurements. We start from the ground state of the system, namely, $|\psi_{\text{in}}\rangle = |E_0\rangle$. The ground state is an eigenstate of Hamiltonian H and nondegenerate, hence, the initial state has no overlap with all the dark states, i.e., $\langle \psi_{\text{in}} | \delta_{k,j} \rangle = \langle E_0 | \delta_{k,j} \rangle = 0$. This is obvious since the energy eigenstates are orthogonal with respect one to another. For the first case, we consider $\tau = 1.2$. The eigenvalues ξ_i of the survival operator $\hat{\mathcal{S}}$ are stationary points of the charge field in Fig. 8. There is a unique maximum $\xi_f \simeq -0.999767$ of the set $\{|\xi_i|\}$ that is closest to the unit circle (see Fig. 8). The system will approach this fixed point when the detection number is large. From Eq. (39), the final state is $|\psi_f\rangle = e^{i\phi_f} |\xi_f^R\rangle$, whose expected energy is $\mathcal{E} = \langle \xi_f^R | H | \xi_f^R \rangle = 0$, while initially the energy is $\mathcal{E}_0 \simeq -2.61313$. The measurements transfer energy to the quantum system continuously until the system reaches its equilibrium state. We present this in Fig. 9.

For the second scenario, we choose $\tau = 1.25$, where there are two eigenvalues $\xi_\alpha \simeq -0.894962 + 0.108282i$ and $\xi_\beta \simeq -0.894962 - 0.108282i$ that are equally close to the unit circle (see Fig. 8). The expected energies of the corresponding eigenstates are $\mathcal{E}_\alpha \simeq 1.46103$ and $\mathcal{E}_\beta \simeq -1.46103$. Clearly, now we have the quantum dynamics presented in Fig. 9. Namely, by periodically collapsing the wave function only on node $|7, 1\rangle$, we drive the whole quantum system and the energy (also other observables) oscillates in time due to

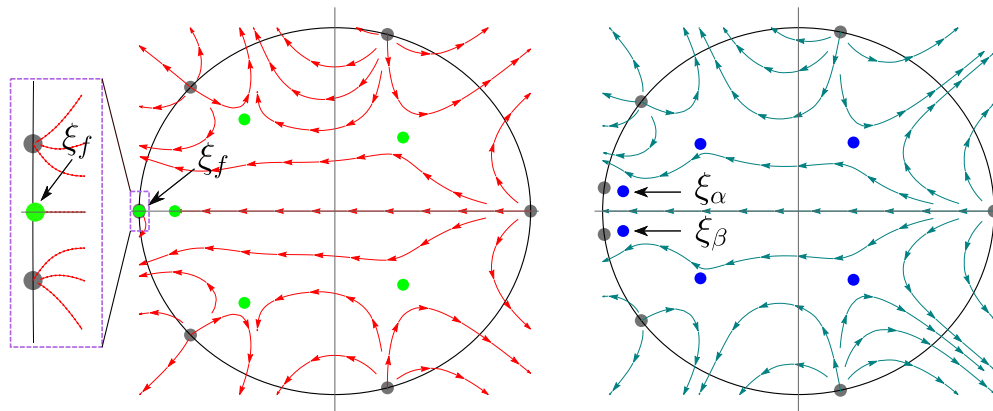


FIG. 8. The classical charge pictures for the eigenvalues of $\hat{\mathcal{G}}$ of G_3 tree model when $\tau = 1.2$ (left) and $\tau = 1.25$ (right). As shown in the figure, when $\tau = 1.2$, there is only one eigenvalue ξ_f that is closest to the unit circle, while at $\tau = 1.25$, two eigenvalues ξ_α and ξ_β that are equally close to the unit circle are found. In the latter case we anticipate quantum dynamics in the long-time limit, while in the former a unique steady state emerges. In this system we have 11 distinct energy levels (see Table I). One would naively expect to find 11 charges; however, some charges vanish, namely, the detected state $|1, 1\rangle$ is orthogonal to some of the energy levels, due to symmetry. As a result, we have 7 charges.

the local measurements. The measurement transfers energy to the quantum system back and forth in an oscillatory way, and the system never reaches a stationary state. These interesting phenomena reveal the effect of the measurements and are also

instructive for the quantum dynamics out of equilibrium. Later on, in Fig. 12, we show such driving can be controlled by the periodicity τ .

2. Selection rule by measurements

Now we consider the cases that the initial state has some overlap with the dark states. According to Eq. (38), the final state of the system is determined by the dark states, which are constructed from the degenerate energy levels. Hence, when the system is driven by measurements, we expect that the nondegenerate eigenenergies will be irrelevant in the long-time limit. Namely, the measurement dynamically selects the degenerate energy levels and wipes out the nondegenerate ones, which effectively is a selection rule. In this part, we exploit the degeneracy of H and explore the selection rule for the degenerate states with the glued tree model.

We first consider the case that the initial state $|\psi_{in}\rangle = (|E_{2,1}\rangle + |E_{10}\rangle)/\sqrt{2}$, which is a linear combination of the degenerate energy level E_2 and nondegenerate energy level E_{10} . The mean energy of the G_3 tree system at the beginning is $\mathcal{E}_0 = E_2/2 + E_{10}/2 \simeq 0.31$. Conditioning the measurements to be null, the system converges to the degenerate energy level only and the component of the nondegenerate energy level is eventually wiped out. So, the expected energy of system in the final state is $\mathcal{E} = E_2 = -2$. In Fig. 10, our numerical simulations show that the energy of the system is indeed E_2 when n is large.

Now we add the component of another degenerate energy level E_5 to the initial state. The initial state then reads as $|\psi_{in}\rangle = (|E_{2,1}\rangle + |E_{10}\rangle + |E_{5,1}\rangle)/\sqrt{3}$. This is a linear combination of two degenerate energy levels and one nondegenerate energy level. Following the selection rule, the two degenerate energy levels determine the final state of the system, and the mean energy of the system will reach the value $\mathcal{E} = -1$ eventually. If we add another nondegenerate energy level E_6 , i.e., $|\psi_{in}\rangle = (|E_{2,1}\rangle + |E_{10}\rangle + |E_{5,1}\rangle + |E_6\rangle)/2$, this does not change the final state, as the selection rule of the measurements wipes out both the $|E_{10}\rangle$ and $|E_6\rangle$ components. We

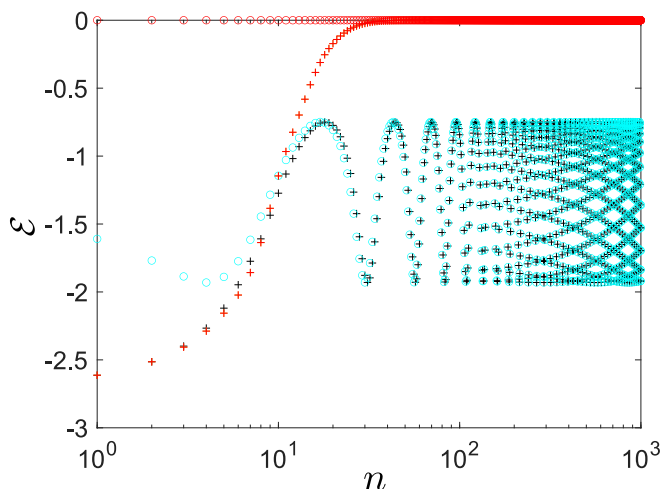


FIG. 9. The expected energy of the G_3 tree system versus the measurement steps n conditioned on all the detections being null. We prepare the system in its ground state ($\langle \mathcal{E} \rangle = -2.61313$), and then perform repeated stroboscopic measurements at the state $|\psi_d\rangle = |1, 1\rangle$ (see Fig. 7). As demonstrated in Fig. 8 when $\tau = 1.2$, there is only a unique eigenvalue ξ_f of $\hat{\mathcal{G}}$ that is closest to the unit circle, corresponding to the state $|\xi_f^R\rangle$, with expected energy $\langle \mathcal{E}_f \rangle = 0$ (red circles). As shown here, the energy of the system (red crosses, numerical simulations) reaches the expected energy when $n \simeq 20$. The detections pump the energy of the system and send it to the new steady state. When $\tau = 1.25$, there are two eigenvalues ξ_α and ξ_β that are equal in magnitude $|\xi_\beta| = |\xi_\alpha|$ (see Fig. 8), while they are also the largest eigenvalues (aside from the dark states which are not relevant due to the initial condition). Now the total energy of the system oscillates. Our theory (cyan circles) predicts this oscillation and perfectly matches the numerical simulations (black crosses) when n is large.

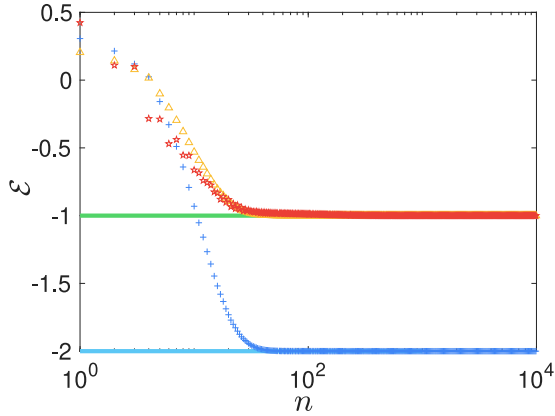


FIG. 10. The expected energy of the G_3 tree system versus the measurement steps n . The blue crosses are numerical simulations for the initial state $|\psi_{\text{in}}\rangle = (|E_{2,1}\rangle + |E_{10}\rangle)/\sqrt{2}$. The selection rule for the final energy of the system indicates that this final energy is the same as that of state $|E_{2,1}\rangle$ since that state belongs to a degenerate subspace, while $|E_{10}\rangle$ does not. The theoretical value of \mathcal{E} in the large- n limit is the blue line. The yellow triangles are for the initial state $|\psi_{\text{in}}\rangle = (|E_{2,1}\rangle + |E_{10}\rangle + |E_{5,1}\rangle)/\sqrt{3}$ (here both $|E_{2,1}\rangle$ and $|E_{5,1}\rangle$ are degenerate, hence the final state is different from the previous case). We also show the mean energy for $|\psi_{\text{in}}\rangle = (|E_{2,1}\rangle + |E_{10}\rangle + |E_{5,1}\rangle + |E_6\rangle)/2$ in red pentagrams. The theoretical predictions of the mean energy \mathcal{E} are the green line. Note that the red and yellow curves merge in the large- n limit. This is because the difference between these two initial conditions is an energy eigenstate which is nondegenerate, and hence unimportant in the long-time limit.

present the numerical simulations in Fig. 10, and the results are consistent with our predictions.

VIII. NULL MEASUREMENTS, INSIGHTS FROM THE CHARGE THEORY

We now provide general insights from the charge theory, which are used to find the largest eigenvalue of $\hat{\mathcal{C}}$ in generic situations. The technique here presented follows, and in some cases extends the ideas in [50,72,73], that were developed in the context of the first detection problem. We consider cases where the dark space is empty, simply because a system with a nonempty dark space can be treated exactly with the tools given in Eq. (8). So, in this section $|\xi_i| < 1$. Furthermore, we consider cases where one or several eigenvalues of the survival operator are close to the unit circle, and hence these are the largest. We develop an approximate expression for the eigenvalue(s), and also give insight into the eigenvectors. We consider four cases: (i) a weak charge scenario, (ii) two charges merging, (iii) triple-charge theory, and finally (iv) quantum Zeno regime, where all the ξ 's approach the unit circle.

A. Weak charge theory

Assume that one of the overlaps denoted p_0 , associated with energy level E_0 , is small, $p_0 \ll 1$, and in particular much smaller than all the others. In the electrostatic language, we have a weak charge at $\exp(-iE_0\tau)$. We find a stationary point

close to this charge, denoted $\xi_f \simeq \exp(-iE_0\tau)$. At ξ_f , the electrostatic force vanishes because the force of the weak charge balances all other forces. By analogy, the stationary point of the Moon-Earth system is much closer to the Moon than to the Earth. Using Eq. (18) together with perturbation theory, we get [72]

$$\xi_f \sim e^{-iE_0\tau} - \epsilon, \quad (47)$$

where

$$\epsilon \sim \frac{p_0}{\sum_{k \neq 0} p_k / (e^{-i\tau E_0} - e^{-i\tau E_k})}. \quad (48)$$

Since $p_0 \ll 1$, $\epsilon \sim 0$. The leading term of ξ_f is $e^{-iE_0\tau}$, hence, $|\xi_f| \sim 1$ and $|\xi_f| < 1$. From Eq. (39), for a system with such a weak charge, the final state is $|\psi_f\rangle \sim e^{i\phi_f} |\xi_f^R\rangle$. Substituting ξ_f into Eq. (19), the expression for the right eigenstate $|\xi_f^R\rangle$ can be highly simplified, which leads to

$$|\psi_f\rangle \sim e^{i\phi_f} |E_0\rangle, \quad (49)$$

where $\phi_f = -i \ln(\xi_f/|\xi_f|) \sim -E_0\tau$. Equation (49) indicates that the final state is the energy eigenstate $|E_0\rangle$. The global phase accumulated is approximately the energy E_0 multiplied by the evolution time. The repeated measurements drive the system to this specific state. To get a deeper understanding of this result, we go back to the definition of the weak charge p_0 , where $p_0 = |\langle \psi_d | E_0 \rangle|^2 \ll 1$. Actually, the ‘‘weakness’’ of the charge means the overlap of the energy state $|E_0\rangle$ and the detection state $|\psi_d\rangle$ is nearly zero, i.e., $\langle \psi_d | E_0 \rangle \sim 0$. Hence, the bright state $|E_0\rangle$ is acting like a nearly dark state, due to the small overlap. The expected energy of the final state is $\langle \mathcal{E} \rangle = \langle \psi_f | H | \psi_f \rangle \sim E_0$.

This picture was demonstrated already in the specific V-shaped system in Sec. VI A. In particular, in this example the weak charge $p_0 \simeq 2.040 \times 10^{-6}$ (note in Sec. VI A, we denoted it p_1). Using Eq. (47), we have $\epsilon \simeq 1.945 \times 10^{-6} - 1.077 \times 10^{-6}i$, from here $\xi_1 \simeq 0.0707353 - 0.997496i$ in excellent agreement with the exact value $\xi_1 = 0.0707353 - 0.997494i$. Moreover, the general equation (49) is directly demonstrated with Eq. (44).

B. Two merging charges

Another mechanism leading to the eigenvalue of $\hat{\mathcal{C}}$ being close to the unit circle is the case when two energy levels, denoted E_a and E_b , satisfy the resonance condition $\exp(-iE_a\tau) \simeq \exp(-iE_b\tau)$ [50]. Note that this can be achieved by modifying τ or some other parameter of H . We then have two charges p_a and p_b close to each other, both located on the unit circle. So we expect to find a stationary point, denoted ξ_f in their neighborhood. This is because the point of zero force is largely determined by this pair. In analogy, the equilibrium point between two neighboring stars is determined to leading order by these and not by other distant stars. An example was shown in Fig. 3(b), however, now we treat the problem in generality. We need to find an approximation for ξ_f as $\delta \rightarrow 0$, where $\delta = (E_b\tau - E_a\tau)/2 \bmod 2\pi$, which measures the angular distance between the two phases. Using Eq. (18), we find [73]

$$\xi_f \sim \frac{p_a e^{-iE_b\tau} + p_b e^{-iE_a\tau}}{p_a + p_b} + O(\delta^2). \quad (50)$$

As shown in Eq. (50), the charges p_a and p_b determine the location of the stationary point ξ_p , and the other charges give only a second-order perturbation. Since $\exp(-iE_a\tau) \simeq \exp(-iE_b\tau)$, $|\xi_f| \sim 1$. As a demonstration of Eq. (50), we consider the charge configuration in Fig. 3(b). Using Eq. (50), we have $\xi_f \simeq -0.8170 + 0.5726i$, while the exact value is $-0.8158 + 0.5722i$. Here $\delta = 0.09$, and the error comes from terms which are second order in δ .

From Eq. (39), the final state of the system then is $|\psi_f\rangle \sim e^{i\phi_f} |\xi_f^R\rangle$. Substituting ξ_f into Eq. (19), we have

$$|\xi_f^R\rangle \sim N(\langle E_b|\psi_d\rangle|E_a\rangle - \langle E_a|\psi_d\rangle|E_b\rangle), \quad (51)$$

where N is for normalization. The eigenstate $|\xi_f^R\rangle$ is a linear combination of the energy eigenstates $|E_a\rangle$ and $|E_b\rangle$ that are close to merging, which is the creation of the Floquet dark state. The expected energy of the final state is

$$\langle \mathcal{E} \rangle \sim \frac{p_b E_a + p_a E_b}{p_a + p_b}. \quad (52)$$

Following the example in Fig. 3(b), we have $\tau = 2$ and the merging charges are $p_0 \simeq 0.108$ and $p_2 \simeq 0.543$ corresponding to the energy levels $E_0 \simeq -1.25$ and $E_2 \simeq 1.80$. Using Eq. (52), the mean energy of the system in the large- n limit is $\mathcal{E} \simeq -0.744$. The exact mean energy is -0.7511 , which is presented in Fig. 4(b).

The global phase accumulated in the measurements is

$$\phi_f \sim -\frac{E_a + E_b}{2}\tau + \frac{p_b - p_a}{p_a + p_b}\delta. \quad (53)$$

The first term on the left-hand side is the leading part of ϕ_f . Like the final state, the phase is also determined by the two merging energy levels.

C. Triple-charge theory

An interesting case is found when three charges merge on the unit circle. In this case we will have two eigenvalues of the survival operator $\hat{\mathcal{C}}$ in the vicinity of these three charges, and in that sense this example is different from those considered in the previous two subsections. Once we have two eigenvalues which have the same magnitude, we expect to find oscillatory behavior, induced by the phase differences, which in turn are controlled in principle by the measurement period τ . For simplicity we consider systems with commensurate energy levels, the three merging energy levels are $E_0 = 0$ and $E_{\pm} = \pm E$ with phases e^0 and $e^{\pm iE\tau} = e^{i2\pi k \pm i\delta}$, where k is an integer and δ is our small parameter. This configuration of charges or phases yields two complex eigenvalues denoted $\xi_{\pm} = r_{\pm} e^{i\theta_{\pm}}$. They are located in the vicinity of the unit circle, as expected from basic electrostatics. We denote $p_0 = |\langle E_0|\psi_d\rangle|^2$ and $p = |\langle E_{\pm}|\psi_d\rangle|^2$. As shown in Appendix D, a third-order expansion of Eq. (18) in δ yields the ξ_+ and ξ_- [72] [see Eqs. (D1) and (D2)]. We find $\xi_+ = \xi_-^*$ up to order $O(\delta^2)$. As mentioned, such a system will yield quantum dynamics even in the long-time limit since other eigenvalues of the survival operator are decaying faster, as they are smaller, which is due to the fact that the three merging charges are situated one next to each other. In principle, the lifetime of these quantum oscillations depends on the other background charges that can break symmetry (to higher order in delta) creating a situation

where one of the eigenvalues ξ_+ or ξ_- is actually closer to the unit circle.

Symmetric background. For symmetric background charges, we have $r_+ = r_-$ and $\theta_+ = -\theta_-$ and, hence, according to our theory, the measurements induce dynamics forever. From Eq. (40), the final state is determined by the states $|\xi_+^R\rangle$ and $|\xi_-^R\rangle$. Using Eq. (19), we have

$$|\xi_+^R\rangle \sim N\left(\frac{\langle E_-|\psi_d\rangle}{C-1}|E_- \rangle + \frac{\langle E_+|\psi_d\rangle}{C+1}|E_+ \rangle + \frac{\langle E_0|\psi_d\rangle}{C}|E_0 \rangle\right), \quad (54)$$

where $C = \sqrt{p_0/(p_0 + 2p)}$. Similarly, $|\xi_-^R\rangle$ reads as

$$|\xi_-^R\rangle \sim N\left(\frac{\langle E_-|\psi_d\rangle}{C+1}|E_- \rangle + \frac{\langle E_+|\psi_d\rangle}{C-1}|E_+ \rangle + \frac{\langle E_0|\psi_d\rangle}{C}|E_0 \rangle\right). \quad (55)$$

Using Eq. (40), since $\theta_+ = -\theta_- = \theta$, the final state of the system is $|\psi_f\rangle = N(a_1 e^{i\theta} |\xi_+^R\rangle + a_2 e^{-i\theta} |\xi_-^R\rangle)$, where a_1 and a_2 are overlaps with the initial state. Specially, we choose $a_1 = a_2$, which leads to

$$|\psi_f\rangle \sim N\{\mathcal{D}(n)\langle E_-|\psi_d\rangle|E_- \rangle + \mathcal{D}^*(n)\langle E_+|\psi_d\rangle|E_+ \rangle - 2 \cos(n\theta)\langle E_0|\psi_d\rangle|E_0 \rangle\}, \quad (56)$$

where $\mathcal{D}(n) = [p_0 \cos(n\theta) + i\sqrt{p_0(p_0 + 2p)} \sin(n\theta)]/p$ and θ is defined by $\xi_+ = r_+ e^{i\theta} = r e^{i\theta}$. Since the first-order approximation of ξ_{\pm} is totally imaginary, when $n \ll 1/\delta^2$, we can express $\theta \sim A\delta$ [$A = \sqrt{p_0/(p_0 + 2p)}$, see Eq. (D3)].

Random background. When the background charges are not strictly symmetric, $|\xi_+| \neq |\xi_-|$. Then, the quantum dynamics will decay away for very large n and the system will go to a fixed state determined by the larger of $|\xi_+|$ and $|\xi_-|$. Nevertheless, the system will exhibit nontrivial dynamics in a certain time regime because of the charge configuration we set (the three charges we consider are symmetric). So the theoretical question is how long will the quantum dynamics last? From the expressions of ξ_+ and ξ_- , we see that $|\xi_+| = |\xi_-|$ up to order $O(\delta^2)$. The background effect comes in order $O(\delta^3)$. So, at least, the quantum dynamics will last until $n \sim 1/\delta^2$. When the number of measurements becomes larger than $1/\delta^2$, the system gradually goes to a fixed state due to the symmetry breaking.

1. Example

To demonstrate the triple-charge theory, we use the glued binary G_3 tree example and tune the measurement time interval τ . As shown in Fig. 11, when $\tau = 2.3$ and 2.35 , we have three charges that are close to each other and far away from other charges (the background charges). As a result, there are two eigenvalues (ξ_+ and ξ_-) of the survival operator that are near the unit circle (orange for $\tau = 2.3$ and red for $\tau = 2.35$ in Fig. 11). Because of the symmetry of the system, they also have the same absolute value, so $|\xi_+| = |\xi_-| \simeq 1$. The exact numerical values, when $\tau = 2.3$, are $|\xi_+| = |\xi_-| = 0.9873$, while using Eqs. (D1) and (D2), we have $|\xi_+| \simeq |\xi_-| \simeq 0.9869$.

The triple-charge configuration leads to persistent quantum dynamics. For instance, the mean energy of the system is driven periodically due to the measurements. Here, we choose

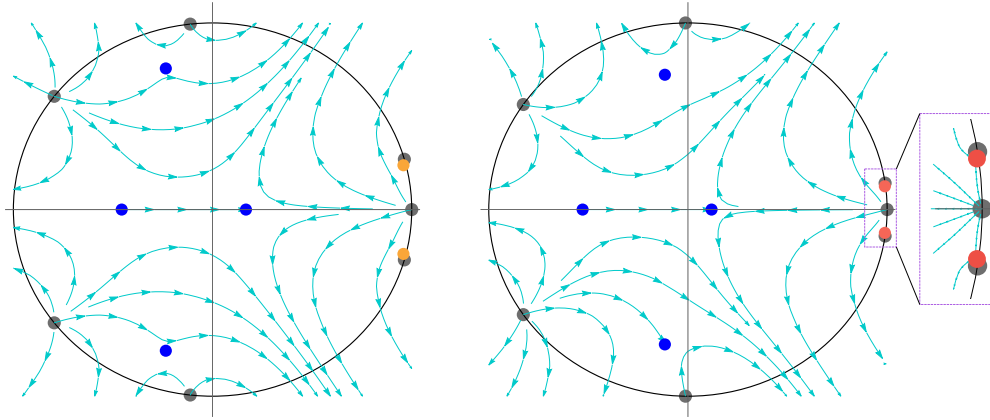


FIG. 11. The classical charge pictures for the eigenvalues of $\hat{\mathcal{C}}$ of the G_3 tree model when $\tau = 2.3$ (left) and $\tau = 2.35$ (right). Here $|\psi_d\rangle = |1, 1\rangle$. As shown in the figure, on the east part, on and just above and below the equator, we see three charges that are close to one another (charges are in gray, on the unit circle). As a result, there are two eigenvalues ξ_+ and ξ_- that are approaching the unit circle and $\xi_+ = \xi_-^*$ (orange for $\tau = 2.3$ and red for $\tau = 2.35$). The other eigenvalues of $\hat{\mathcal{C}}$, in the unit disk, are colored blue. They will not contribute to the long-time limit as they are further away from the unit circle. Similar to Fig. 8, some of the charges in this system are zero, hence, while the number of distinct energy levels is 11 (Table I) the number of nonzero charges is 7.

the initial state to be the ground state, where the effects of the dark states can be neglected. As shown in Fig. 12, the mean energy of the G_3 system oscillates periodically with the number of measurement steps n and our theory (lines) fits the numerical simulations (crosses). More importantly, the oscillation frequency of the mean energy changes when we change τ . As shown in the figure, the oscillation frequency at $\tau = 2.3$ is faster than the frequency at $\tau = 2.35$. This follows from the charge picture, as the relative phase, i.e., $\text{Arg}(\xi_+) - \text{Arg}(\xi_-)$, at $\tau = 2.3$ is larger than that at $\tau = 2.35$ (see Fig. 11). The oscillation frequency is controlled by this relative phase, and hence the frequency at $\tau = 2.3$ is faster.

D. Quantum Zeno regime

As we increase the number of charges merging to the vicinity of a point on the unit circle, more eigenvalues of the survival operator approach the unit circle, and they are also all close to each other. An example is the quantum Zeno regime [89–96], where $\tau \sim 0$ and all phases $\exp(-iE_k\tau)$ coalesce [as an example, see Fig. 3(a)]. In the quantum Zeno regime, due to the fast measurements, the dynamics of the monitored system is slowed down [96] and our goal is to characterize this behavior. In general, we have a set of eigenvalues of the survival operator (excluding the trivial one on zero) and we consider their absolute value $|\xi_1|, |\xi_2|, \dots, |\xi_w|$, which are approaching unity as $\tau \sim 0$. The fastest decay mode is given by the minimum of the set $|\xi_{\min}|$. Our goal is to find a rough estimate for this eigenvalue, controlling the rate of the decay of this component $|\xi_{\min}|^n$ [see Eq. (36)].

Basic electrostatics tells us that all the stationary points are located in the convex hull of the charges [50], the area of which vanishes as $\tau \sim 0$. We use this to our advantage and obtain a lower bound for $|\xi|$:

$$|\xi_{\min}| \geq \cos(\Delta E \tau / 2), \quad (57)$$

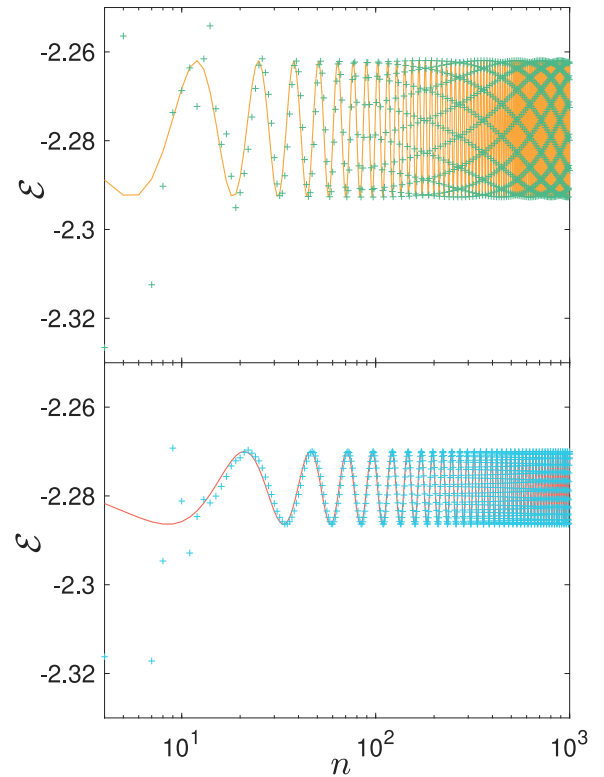


FIG. 12. The mean energy of G_3 tree system versus the measurement steps n . Initially, the system is at its ground state. The measurements drive the mean energy of the system periodically. The upper plot is for $\tau = 2.3$, where the green crosses are numerical simulations and the orange line is the theory. The lower plot is for $\tau = 2.35$, and the theory (red line) perfectly matches the numerical simulations (blue pentagrams). The oscillation frequency at $\tau = 2.3$ is faster than the frequency at $\tau = 2.35$ because the relative phase of ξ_+ and ξ_- at $\tau = 2.3$ is larger than the phase at $\tau = 2.35$ (see Fig. 11).

where ΔE is the width of the energy spectrum, namely, $\Delta E = E_{\max} - E_{\min}$. An example of Eq. (57) is Eq. (42) for the three-level system, which is demonstrated in Fig. 3(f). Then we let $|\xi_{\min}|^{n_b} = e^{-1}$, which leads to $n_b = -1/\ln[\cos(\Delta E \tau/2)]$. The lower bound of the evolution time $t_b = n_b \tau$ is

$$t_b \sim \frac{-\tau}{\ln[\cos(\Delta E \tau/2)]} \sim \frac{8}{(\Delta E)^2 \tau}. \quad (58)$$

From Eq. (58), the evolution of the system is repressed, and the lower bound t_b is proportional to τ^{-1} . The width of the energy band also affects this lower bound. The bound of the number of measurements then is $n_b = t_b/\tau$, which is proportional to τ^{-2} . So when $\tau \sim 0$, the relaxation is therefore extremely slow [see example in Fig. 4(a)].

IX. EXCEPTIONAL POINTS

Previously in Sec. III C we presented a simple example of an exceptional point of a two-level system. We now briefly explain how similar effects can be found in larger systems. In particular, we are searching for cases where all the eigenvalues of survival operator $\xi = 0$. Then, clearly, the right-hand side of our main Eq. (36) is equal to zero and the whole approach is invalid. As mentioned, this corresponds to a situation where we cannot satisfy the condition of null measurements to begin with.

The basic question is how to construct such systems. Here the charge picture is very useful. Consider a three-level system. Then, if we have three charges of the same magnitude on -120° , 0 , and 120° on the unit circle, clearly from symmetry all the eigenvalues of $\hat{\mathcal{C}}$ are zero. This is because the stationary point of this charge configuration is in the center of the unit disk. Assume this system has energy levels $-E$, 0 , E , and further assume that corresponding wave functions have the same overlaps with the detected state (so the charges are the same). In this case, if we choose $E\tau = 2\pi/3 + 2\pi k$ with k an integer, we get a charge configuration that will exhibit the desired result. It is now rather easy to construct a Hamiltonian that meets this demand, and we present an example below. In fact, this method can be extended to systems beyond three- or two-level systems rather easily.

We also note that one may have an exceptional point that is generated from the degeneracy of a few (not all) eigenvalues of the survival operator. Physically, this corresponds to the phenomena where the unitary evolution and measurements can not reach a steady state given in Eq. (39) because of the loss of dimensionality of the survival operator. To see that, let us consider the case where two eigenvalues ξ_i and ξ_j are degenerate, i.e., $\xi_i = \xi_j$. Using Eqs. (20) and (25), the right and left eigenvectors also become parallel, namely, $|\xi_i^R\rangle = |\xi_j^R\rangle$ and $\langle \xi_i^L| = \langle \xi_j^L|$. In other words, the dimension of the survival operator is effectively reduced by one, and there exists one state, we denote it $|\xi_E\rangle$, which cannot be expanded in the eigenbasis of $\hat{\mathcal{C}}$. Furthermore, $|\xi_E\rangle$ is not an eigenmode of $\hat{\mathcal{C}}$. Because of that, when we apply our protocol to this state, namely $N\hat{\mathcal{C}}^n|\xi_E\rangle$, even in the long-time limit, the measurements cannot drive the system into the steady state as in Eq. (39).

Remark. In the dark subspace, the eigenvalues $\exp(-iE_k\tau)$ of the survival operator $\hat{\mathcal{C}}$ are $(g_k - 1)$ -fold degenerate. When

$g_k \geq 3$, using Eq. (8), there are two or more eigenstates $|\delta_{k,i}\rangle$ of the survival operator $\hat{\mathcal{C}}$. As they are constructed by a Gram-Schmidt procedure, these dark states are orthogonal. Using Eqs. (19) and (24), for the eigenstates of $\hat{\mathcal{C}}$ that correspond to the eigenvalues that lie in the unit disk, i.e., $0 < |\xi| < 1$, when two ξ 's coalesce, both left and right eigenvectors become parallel. Thus, we only have one eigenvector instead of two.

A. Example

Here we find the Hamiltonian of the three-level system with the approach mentioned above. As mentioned, we want the three charges to be located on angles -120° , 0 , and 120° . This can be easily achieved by choosing equally spaced energy levels, for instance, $E_0 = -\gamma$, $E_1 = 0$, and $E_2 = \gamma$, where $\gamma > 0$. When $\tau\gamma = 2\pi/3 + 2\pi k$, we get the desired charge configuration.

The second step is to have all three charges with equal magnitude, i.e., $p_0 = p_1 = p_2 = \frac{1}{3}$. We choose the detection state $|\psi_d\rangle = (1, 0, 0)^T$. We then construct a group of orthogonal eigenstates of H that $|\langle \psi_d | E_i \rangle|^2 = \frac{1}{3}$. A possible choice of such eigenstates $|E_i\rangle$ is $|E_0\rangle = (1/\sqrt{3}, -1/\sqrt{6}, 1/\sqrt{2})^T$, $|E_1\rangle = (-1/\sqrt{3}, 1/\sqrt{6}, 1/\sqrt{2})^T$, and $|E_2\rangle = (1/\sqrt{3}, \sqrt{2/3}, 0)^T$. Such eigenstates of H have identical overlaps with the detection state, and hence all the charges have the same magnitude.

The last step is to find the concrete form of H . Since $|E_i\rangle$ is an eigenstate of H with eigenvalues E_i , we have $H|E_i\rangle = E_i|E_i\rangle$, which leads to

$$H = -\gamma \begin{pmatrix} 0 & -1/\sqrt{2} & 1/\sqrt{6} \\ -1/\sqrt{2} & -1/2 & -1/(2\sqrt{3}) \\ 1/\sqrt{6} & -1/(2\sqrt{3}) & 1/2 \end{pmatrix}. \quad (59)$$

For a quantum system with such a Hamiltonian, when $\tau\gamma = 2\pi/3 + 2\pi k$, we cannot satisfy the condition of null measurements. In other words, the system is detected with probability one by the local measurements. $\xi = 0$ is an exceptional point of the survival operator of order three. With the same procedure, this can be generalized for larger systems.

X. SUMMARY

We have investigated the properties of the quantum survival operator $\hat{\mathcal{C}}$, which in turn gives the state of the system after a large number of conditional measurements. We have classified six types of generic behaviors:

(1) In the presence of symmetry of the Hamiltonian and hence an energy spectrum which is degenerate, the system will exhibit dynamics determined by the energy levels of the systems. However, only the degenerate energy levels participate, i.e., the measurements select a subclass of states. Of course, this is the case under the condition that initially $|\psi_{\text{in}}\rangle$ has some overlap with the dark sector of the Hilbert space.

(2) We also find Floquet dark states that are inherently related to periodic driving. By choosing the period τ defined in Eq. (9), one can drive a system into a dark state independent of the symmetry of a specific system. While for effect 1 we must demand certain symmetry of the system that

gives rise to energy degeneracy, we may use Floquet dark states for any system. In other words, with periodic driving, we can engineer dark states for practically any quantum system.

(3) In the absence of a dark subspace, for example, for systems with no degeneracy, e.g., interacting or chaotic systems, and when τ is chosen in such a way that we have no Floquet dark states, a different physical mechanism emerges. Typically, the final state of the system is unique. This means that in the long-time limit, we have no dynamics at all, and we can say that the system reaches a kind of equilibrium, induced by the periodic null measurements. This state corresponds the eigenvalue of the non-Hermitian survival operator that is closest to the unit circle. In the second part of the paper we developed tools to identify this state and these are based on the classical charge theory initially promoted in Refs. [50,51].

(4) Under certain conditions, we find a pair of eigenvalues of $\hat{\mathcal{S}}$ which together are the largest in magnitude. However, their magnitude is less than unity (dark states have eigenvalues equal unity). We find that these eigenvalues then have a relative phase that is controlled by the rate $1/\tau$ [see Eq. (40)]. In this case, the system exhibits oscillation controlled by the measurements, which is promising for the quantum operation. Such an oscillation can be achieved even for relatively large systems, like the glued tree example. One can also easily control the oscillation frequency and amplitude by tuning the measurement rate, as shown in Fig. 12.

(5) In the Zeno limit, all the eigenvalues of $\hat{\mathcal{S}}$ approach the unit circle. This means that oscillations are effectively undetectable, and the relaxations are slow (as is well known). We have presented a lower bound for the eigenvalues of the survival operator, showing their vicinity to the unit circle. In this case, when the initial condition does not overlap with the detected state and in the limit $\tau \rightarrow 0$, null measurements are found with probability one, even in the absences of conditioning.

(6) An interesting case is a situation where all the eigenvalues of $\hat{\mathcal{S}}$ are equal to zero. This corresponds to the exceptional point of the non-Hermitian survival operator. The physics in this case implies that the condition of null measurements is not realizable (in that sense it is the complete opposite of the Zeno regime). Rather, the system is detected with probability one by the local measurements, and hence the condition we impose is violated. Also, this effect is inherent to the periodicity of the measurements, and cannot be found if the measurements are at random times. The classical charge picture was proven to be very useful here, in the sense that we can exploit the symmetry of the charge picture to direct the eigenvalues of $\hat{\mathcal{S}}$ to a unique stable point in the center of the unit disk, and hence exhibit the exceptional physics.

The theory developed here, in particular the charge theory, makes it possible to realize the long-time behavior using an intuitive electrostatic analogy. For example, a single weak charge, corresponding to a weak overlap of a stationary energy state with the detected state, or merging charges (phases) on the unit circle, imply an eigenvalue of $\hat{\mathcal{S}}$ which is close to unity in magnitude, and its precise value can be estimated in generality. Maybe more interesting is the merging of three charges on the unit circle (see Fig. 11) since here we get two

eigenvalues of $\hat{\mathcal{S}}$ approaching the unit charges, and then we get the dynamical effect due to the phase difference (effect 4). These effects were explored with the glued tree example (see Fig. 12). Clearly, the high degree of symmetry in this case, and the energy degeneracy of the system, imply a large dark subspace and, hence, this type of example exhibits physical behaviors drastically different from the simple three-level systems. As mentioned, the charge picture is used also to find a lower bound for the Zeno limit, and helps tremendously in the identification of exceptional points.

ACKNOWLEDGMENT

The support of Israel Science Foundation's Grant No. 1614/21 as well as the support by the Julian Schwinger Foundation (K.Z.) are acknowledged.

APPENDIX A: MATRIX DETERMINANT LEMMA

In this Appendix, we present the details for the calculation using the matrix determinant lemma. The formula of the matrix determinant lemma is

$$\det(A + uv^T) = (1 + v^T A^{-1} u) \det(A), \quad (\text{A1})$$

where A is an invertible square matrix and u, v are column vectors. For the eigenvalues of the survival operator $\hat{\mathcal{S}}$, we have

$$\det(\xi - \hat{\mathcal{S}}) = \det[\xi - \hat{U}(\tau) + |\psi_d\rangle\langle\psi_d|\hat{U}(\tau)]. \quad (\text{A2})$$

We let $A = \xi - \hat{U}(\tau)$, $u = |\psi_d\rangle$, and $v^T = \langle\psi_d|\hat{U}(\tau)$, which leads to

$$\det(\xi - \hat{\mathcal{S}}) = \det[\xi - \hat{U}(\tau)] \langle\psi_d|[\xi - \hat{U}(\tau)]^{-1}|\psi_d\rangle \xi. \quad (\text{A3})$$

This is the formula we used in the main text.

APPENDIX B: CALCULATION FOR THE RIGHT EIGENVECTORS OF SURVIVAL OPERATOR WITH EIGENVALUES IN THE UNIT DISK

In this Appendix, we present the details for Eq. (19) in the main text. As discussed in the main text, we expand the right eigenstates in the bright subspace

$$|\xi^R\rangle = \sum_{\{B\}} a_i |\beta_i\rangle, \quad (\text{B1})$$

where a_i is the index we are looking for and $\{B\}$ represents the summation in the bright subspace. Substituting Eq. (B1) into (3), we have

$$\hat{\mathcal{S}}|\xi^R\rangle = \sum_{\{B\}} a_i (1 - D)\hat{U}(\tau)|\beta_i\rangle \quad (\text{B2})$$

$$= \sum_{\{B\}} a_i (1 - D)e^{-i\tau E_i} |\beta_i\rangle \quad (\text{B3})$$

$$= \xi \sum_{\{B\}} a_i |\beta_i\rangle. \quad (\text{B4})$$

Multiplying Eqs. (B3) and (B4) by $\langle\beta_j|$, we have

$$\xi a_j = \sum_{\{B\}} a_i e^{-i\tau E_i} \langle\beta_j|(1 - D)|\beta_i\rangle. \quad (\text{B5})$$

Following the definition of the charges, the matrix elements on the right-hand side of Eq. (B5) can be simplified:

$$\langle \beta_j | (1 - D) | \beta_i \rangle = \begin{cases} 1 - \langle \beta_j | D | \beta_j \rangle = 1 - p_j, & i = j \\ -\langle \beta_j | D | \beta_i \rangle = -\sqrt{p_j p_i}, & i \neq j. \end{cases} \quad (\text{B6})$$

Substituting Eq. (B6) into (B5), we have

$$\sum_{\{B\}, i \neq j} a_i e^{-i\tau E_i} \sqrt{p_i} = a_j \frac{[e^{-i\tau E_j} (1 - p_j) - \xi_j]}{\sqrt{p_j}}. \quad (\text{B7})$$

Now we define $b_i = a_i e^{-i\tau E_i} \sqrt{p_i}$, so $a_i = b_i / (e^{-i\tau E_i} \sqrt{p_i})$. We also define $\zeta_j = 1 - (1 - e^{i\tau E_j} \xi_j) / p_j$. Equation (B7) then can be simplified as

$$\sum_{\{B\}, i \neq j} b_i = b_j \zeta_j. \quad (\text{B8})$$

For $j = 1, 2, \dots, w$, Eq. (B8) is an equation set, which contains w terms. We want to rewrite this equation set into the matrix form. We define the vector B as

$$B^\dagger = (b_1^*, b_2^*, \dots, b_w^*). \quad (\text{B9})$$

Then, the matrix is

$$M = \begin{Bmatrix} \zeta_1 & 1 & 1 & \dots & 1 \\ 1 & \zeta_2 & 1 & \dots & 1 \\ 1 & 1 & \zeta_3 & \dots & 1 \\ \vdots & \vdots & \vdots & \ddots & \vdots \\ 1 & 1 & 1 & \dots & \zeta_w \end{Bmatrix}. \quad (\text{B10})$$

Equation (B8) then can be rewritten as

$$MB = 0. \quad (\text{B11})$$

Using Eq. (B11) or (B8), we have

$$b_i = b_1 \frac{\zeta_1 - 1}{\zeta_i - 1}. \quad (\text{B12})$$

Substituting Eq. (B12) into the expressions for b_i and ζ_i , we get the expression for a_i :

$$a_i = a_1 \sqrt{\frac{p_i}{p_1}} \frac{e^{-i\tau E_1} - \xi}{e^{-i\tau E_i} - \xi} = \frac{a_1 (e^{-i\tau E_1} - \xi)}{\sqrt{p_1}} \frac{\sqrt{p_i}}{e^{-i\tau E_i} - \xi}. \quad (\text{B13})$$

From Eq. (B13), we see that a_2, a_3, \dots, a_w can be expressed by the a_1 . We can choose a_1 freely, and in the end it is a global

constant that can be neglected by the normalization. Here we choose

$$a_1 = \frac{\sqrt{p_1}}{e^{-i\tau E_1} - \xi}, \quad \text{then } a_i = \frac{\sqrt{p_i}}{e^{-i\tau E_i} - \xi}. \quad (\text{B14})$$

Using Eq. (B1), we have

$$|\xi^R\rangle = \sum_{\{B\}} \frac{\sqrt{p_i}}{e^{-i\tau E_i} - \xi} |\beta_i\rangle. \quad (\text{B15})$$

Using Eq. (11), the bright states $|\beta_i\rangle = \hat{P}_i |\psi_d\rangle / \sqrt{p_i}$. So, together with Eq. (B15) we have

$$|\xi^R\rangle = \sum_{i=1}^w \frac{\hat{P}_i}{e^{-i\tau E_i} - \xi} |\psi_d\rangle. \quad (\text{B16})$$

APPENDIX C: RELATION BETWEEN RIGHT AND LEFT EIGENSTATES

In this Appendix we derive a relation that connects the right eigenvectors to the left eigenvectors. Using Eqs. (20) and (25), we find the right and left eigenstates can be related:

$$\hat{U}(\tau) |\xi^R\rangle = |\xi^L\rangle^*, \quad (\text{C1})$$

where $*$ is the complex conjugate. For a two-level system, if $|\xi^L\rangle = \{a + ib, c + id\}^T$ (a, b, c, d are real numbers), then $|\xi^L\rangle^* = \{a - ib, c - id\}^T$. Equation (C1) shows that the evolution operator $\hat{U}(\tau)$ maps the right eigenstate of survival operator $\hat{\mathcal{C}}$ to the corresponding left one.

APPENDIX D: TRIPLE-CHARGE THEORY

In this Appendix we present the approximate expressions of ξ_+ and ξ_- for the triple-charge theory. The perturbation approach applied here is that we perform a third-order expansion of Eq. (18) in small parameter δ . The eigenvalues ξ_+ and ξ_- then read as

$$\xi_+ = r_+ e^{i\theta_+} \sim 1 + iA\delta - B\delta^2 + O(\delta^3), \quad (\text{D1})$$

$$\xi_- = r_- e^{-i\theta_-} \sim 1 - iA\delta - B\delta^2 + O(\delta^3), \quad (\text{D2})$$

where

$$A = \sqrt{\frac{p_0}{p_0 + 2p}}, \quad (\text{D3})$$

$$B = \frac{p_0 + p}{2p_0 + 4p} - \frac{p}{(p_0 + 2p)^2} \sum_{j \neq 0, \pm} \frac{p_j}{1 - e^{-iE_j \tau}}. \quad (\text{D4})$$

- [1] H. Rabitz, R. de Vivie-Riedle, M. Motzkus, and K. Kompa, Whither the future of controlling quantum phenomena? *Science* **288**, 824 (2000).
- [2] A. Baksic, H. Ribeiro, and A. A. Clerk, Speeding up Adiabatic Quantum State Transfer by Using Dressed States, *Phys. Rev. Lett.* **116**, 230503 (2016).
- [3] X. Wang, M. Allegra, K. Jacobs, S. Lloyd, C. Lupo, and M. Mohseni, Quantum Brachistochrone Curves as Geodesics: Obtaining Accurate Minimum-Time Protocols for the

- Control of Quantum Systems, *Phys. Rev. Lett.* **114**, 170501 (2015).
- [4] A. del Campo and K. Sengupta, Controlling quantum critical dynamics of isolated systems, *Eur. Phys. J.: Spec. Top.* **224**, 189 (2015).
- [5] D. Guéry-Odelin, A. Ruschhaupt, A. Kiely, E. Torrontegui, S. Martínez-Garaot, and J. G. Muga, Shortcuts to adiabaticity: Concepts, methods, and applications, *Rev. Mod. Phys.* **91**, 045001 (2019).

- [6] R. Uola, A. C.S. Costa, H. C. Nguyen, and O. Gühne, Quantum steering, *Rev. Mod. Phys.* **92**, 015001 (2020).
- [7] L. M. K. Vandersypen and I. L. Chuang, Nmr techniques for quantum control and computation, *Rev. Mod. Phys.* **76**, 1037 (2005).
- [8] R. Islam, E. E. Edwards, K. Kim, S. Korenblit, C. Noh, H. Carmichael, G.-D. Lin, L.-M. Duan, C.-C. Joseph Wang, J.K. Freericks, and C. Monroe, Onset of a quantum phase transition with a trapped ion quantum simulator, *Nat. Commun.* **2**, 377 (2011).
- [9] C. Senko, P. Richerme, J. Smith, A. Lee, I. Cohen, A. Retzker, and C. Monroe, Realization of a Quantum Integer-Spin Chain with Controllable Interactions, *Phys. Rev. X* **5**, 021026 (2015).
- [10] L. Magrini, P. Rosenzweig, C. Bach, A. Deutschmann-Olek, S. G. Hofer, S. Hong, N. Kiesel, A. Kugi, and M. Aspelmeyer, Real-time optimal quantum control of mechanical motion at room temperature, *Nature (London)* **595**, 373 (2021).
- [11] R. Barends, A. Shabani, L. Lamata, J. Kelly, A. Mezzacapo, U. Las Heras, R. Babbush, A. G. Fowler, B. Campbell, Yu Chen, Z. Chen, B. Chiaro, A. Dunsworth, E. Jeffrey, E. Lucero, A. Megrant, J. Y. Mutus, M. Neeley, C. Neill, P. J. J. O'Malley *et al.*, Digitized adiabatic quantum computing with a superconducting circuit, *Nature (London)* **534**, 222 (2016).
- [12] M. A. Nielsen and I. L. Chuang, *Quantum Computation and Quantum Information: 10th Anniversary Edition* (Cambridge University Press, Cambridge, 2010)
- [13] M. Shapiro and P. Brumer, *Quantum Control of Molecular Processes* (Wiley, Hoboken, NJ, 2012).
- [14] M. S. Rudner, N. H. Lindner, E. Berg, and M. Levin, Anomalous Edge States and the Bulk-Edge Correspondence for Periodically Driven Two-Dimensional Systems, *Phys. Rev. X* **3**, 031005 (2013).
- [15] P. Titum, N. H. Lindner, M. C. Rechtsman, and G. Refael, Disorder-Induced Floquet Topological Insulators, *Phys. Rev. Lett.* **114**, 056801 (2015).
- [16] M. M. Roses, H. Landa, and E. G. Dalla Torre, Simulating long-range hopping with periodically driven superconducting qubits, *Phys. Rev. Res.* **3**, 033288 (2021).
- [17] A. Solfanelli, L. Buffoni, A. Cuccoli, and M. Campisi, Maximal energy extraction via quantum measurement, *J. Stat. Mech.* (2019) 094003.
- [18] L. Buffoni, A. Solfanelli, P. Verrucchi, A. Cuccoli, and M. Campisi, Quantum Measurement Cooling, *Phys. Rev. Lett.* **122**, 070603 (2019).
- [19] D. K. Burgarth, P. Facchi, V. Giovannetti, H. Nakazato, S. Pascazio, and K. Yuasa, Exponential rise of dynamical complexity in quantum computing through projections, *Nat. Commun.* **5**, 5173 (2014).
- [20] M. H. Mohammady and A. Romito, Conditional work statistics of quantum measurements, *Quantum* **3**, 175 (2019).
- [21] A. Riera-Campeny, J. Ollé, and A. Masó-Puigdellosas, Measurement-induced resetting in open quantum systems, [arXiv:2011.04403](https://arxiv.org/abs/2011.04403).
- [22] S. Roy, J. T. Chalker, I. V. Gornyi, and Y. Gefen, Measurement-induced steering of quantum systems, *Phys. Rev. Res.* **2**, 033347 (2020).
- [23] D. V. Vasilyev, A. Grankin, M. A. Baranov, L. M. Sieberer, and P. Zoller, Monitoring quantum simulators via quantum non-demolition couplings to atomic clock qubits, *PRX Quantum* **1**, 020302 (2020).
- [24] B. Skinner, J. Ruhman, and A. Nahum, Measurement-Induced Phase Transitions in the Dynamics of Entanglement, *Phys. Rev. X* **9**, 031009 (2019).
- [25] A. Nahum, S. Roy, B. Skinner, and J. Ruhman, Measurement and entanglement phase transitions in all-to-all quantum circuits, on quantum trees, and in landau-ginsburg theory, *PRX Quantum* **2**, 010352 (2021).
- [26] A. Lavasani, Y. Alavirad, and M. Barkeshli, Measurement-induced topological entanglement transitions in symmetric random quantum circuits, *Nat. Phys.* **17**, 342 (2021).
- [27] Y. Bao, S. Choi, and E. Altman, Symmetry enriched phases of quantum circuits, *Ann. Phys. (N.Y.)* **435**, 168618 (2021).
- [28] S. Sang and T. H. Hsieh, Measurement Protected Quantum Phases, *Phys. Rev. Res.* **3**, 023200 (2021).
- [29] M. Wampler, B. J. J. Khor, G. Refael, and I. Klich, Stirring by staring: Measurement induced chirality, [arXiv:2108.05906](https://arxiv.org/abs/2108.05906).
- [30] M. B. Plenio and P. L. Knight, The quantum-jump approach to dissipative dynamics in quantum optics, *Rev. Mod. Phys.* **70**, 101 (1998).
- [31] T. Müller, S. Diehl, and M. Buchhold, Measurement-Induced Dark State Phase Transitions in Long-Ranged Fermion Systems, *Phys. Rev. Lett.* **128**, 010605 (2022).
- [32] Z. K. Mineev, S. O. Mundhada, S. Shankar, P. Reinhold, R. Gutiérrez-Jáuregui, R. J. Schoelkopf, M. Mirrahimi, H. J. Carmichael, and M. H. Devoret, To catch and reverse a quantum jump mid-flight, *Nature (London)* **570**, 200 (2019).
- [33] Xhek Turkeshi, Alberto Biella, Rosario Fazio, Marcello Dalmonte, and Marco Schiró, Measurement-induced entanglement transitions in the quantum ising chain: From infinite to zero clicks, *Phys. Rev. B* **103**, 224210 (2021).
- [34] A. Biella and M. Schiró, Many-Body Quantum Zeno Effect and Measurement-Induced Subradiance Transition, *Quantum* **5**, 528 (2021).
- [35] F. Minganti, A. Miranowicz, R. W. Chhajlany, I. I. Arkhipov, and F. Nori, Hybrid-liouvillian formalism connecting exceptional points of non-Hermitian hamiltonians and liouvillians via postselection of quantum trajectories, *Phys. Rev. A* **101**, 062112 (2020).
- [36] P. Kumar, K. Snizhko, and Y. Gefen, Near-unit efficiency of chiral state conversion via hybrid-liouvillian dynamics, *Phys. Rev. A* **104**, L050405 (2021).
- [37] S. Gopalakrishnan and M. J. Gullans, Entanglement and Purification Transitions in Non-Hermitian Quantum Mechanics, *Phys. Rev. Lett.* **126**, 170503 (2021).
- [38] S.-K. Jian, Z.-C. Yang, Z. Bi, and X. Chen, Yang-lee edge singularity triggered entanglement transition, *Phys. Rev. B* **104**, L161107 (2021).
- [39] J Preskill, Quantum Computing in the NISQ era and beyond, *Quantum* **2**, 79 (2018).
- [40] C. Monroe, W. C. Campbell, L.-M. Duan, Z.-X. Gong, A. V. Gorshkov, P. W. Hess, R. Islam, K. Kim, N. M. Linke, G. Pagano, P. Richerme, C. Senko, and N. Y. Yao, Programmable quantum simulations of spin systems with trapped ions, *Rev. Mod. Phys.* **93**, 025001 (2021).
- [41] Qiskit Development Team, Quantum computing.
- [42] Honeywell International Inc., Honeywell system model h1.
- [43] S. Fishman, D. R. Grempel, and R. E. Prange, Chaos, Quantum Recurrences, and Anderson Localization, *Phys. Rev. Lett.* **49**, 509 (1982).

- [44] N. Moiseyev, *Non-Hermitian Quantum Mechanics* (Cambridge University Press, Cambridge, 2011).
- [45] R. El-Ganainy, K. G. Makris, M. Khajavikhan, Z. H. Musslimani, S. Rotter, and D. N. Christodoulides, Non-Hermitian physics and PT symmetry, *Nat. Phys.* **14**, 11 (2018).
- [46] Y. Ashida, Z. Gong, and M. Ueda, Non-Hermitian physics, *Adv. Phys.* **69**, 249 (2020).
- [47] H. Mabuchi and P. Zoller, Inversion of Quantum Jumps in Quantum Optical Systems under Continuous Observation, *Phys. Rev. Lett.* **76**, 3108 (1996).
- [48] S. Gao, Lindblad approach to quantum dynamics of open systems, *Phys. Rev. B* **57**, 4509 (1998).
- [49] C. Gardiner, P. Zoller, and P. Zoller, *Quantum Noise: A Handbook of Markovian and Non-Markovian Quantum Stochastic Methods with Applications to Quantum Optics*, Springer Series in Synergetics (Springer, Berlin, 2004).
- [50] F. A. Grünbaum, L. Velázquez, A. H. Werner, and R. F. Werner, Recurrence for discrete time unitary evolutions, *Commun. Math. Phys.* **320**, 543 (2013).
- [51] J. Bourgain, F. A. Grünbaum, L. Velázquez, and J. Wilkening, Quantum recurrence of a subspace and operator-valued schur functions, *Commun. Math. Phys.* **329**, 1031 (2014).
- [52] B. Höckendorf, A. Alvermann, and H. Fehske, Topological origin of quantized transport in non-Hermitian floquet chains, *Phys. Rev. Res.* **2**, 023235 (2020).
- [53] T. T. Koutserimpas and R. Fleury, Nonreciprocal Gain in Non-Hermitian Time-Floquet Systems, *Phys. Rev. Lett.* **120**, 087401 (2018).
- [54] Z. Papić, Weak ergodicity breaking through the lens of quantum entanglement, [arXiv:2108.03460](https://arxiv.org/abs/2108.03460).
- [55] F. Thiel, I. Mualem, D. Meidan, E. Barkai, and D. A. Kessler, Dark states of quantum search cause imperfect detection, *Phys. Rev. Res.* **2**, 043107 (2020).
- [56] T. Kato, *Perturbation Theory for Linear Operators*, Classics in Mathematics (Springer, Berlin, 1995), Vol. 132.
- [57] W. D. Heiss, Phases of wave functions and level repulsion, *Eur. Phys. J. D* **7**, 1 (1999).
- [58] M. V. Berry, Physics of Non-Hermitian Degeneracies, *Czech. J. Phys.* **54**, 1039 (2004).
- [59] E. Persson, I. Rotter, H.-J. Stöckmann, and M. Barth, Observation of Resonance Trapping in an Open Microwave Cavity, *Phys. Rev. Lett.* **85**, 2478 (2000).
- [60] C. Dembowski, H.-D. Gräf, H. L. Harney, A. Heine, W. D. Heiss, H. Rehfeld, and A. Richter, Experimental Observation of the Topological Structure of Exceptional Points, *Phys. Rev. Lett.* **86**, 787 (2001).
- [61] K. G. Makris, R. El-Ganainy, D. N. Christodoulides, and Z. H. Musslimani, Beam Dynamics in \mathcal{PT} Symmetric Optical Lattices, *Phys. Rev. Lett.* **100**, 103904 (2008).
- [62] S. Klaiman, U. Günther, and N. Moiseyev, Visualization of Branch Points in \mathcal{PT} -Symmetric Waveguides, *Phys. Rev. Lett.* **101**, 080402 (2008).
- [63] B. Zhen, C. W. Hsu, Y. Igarashi, L. Lu, I. Kammer, A. Pick, S. Chua, J. D. Joannopoulos, and M. Soljačić, Spawning rings of exceptional points out of Dirac cones, *Nature (London)* **525**, 354 (2015).
- [64] A. Cerjan, A. Raman, and S. Fan, Exceptional Contours and Band Structure Design in Parity-Time Symmetric Photonic Crystals, *Phys. Rev. Lett.* **116**, 203902 (2016).
- [65] P. Facchi and S. Pascazio, Quantum zeno dynamics: mathematical and physical aspects, *J. Phys. A: Math. Theor.* **41**, 493001 (2008).
- [66] F. Schäfer, I. Herrera, S. Cherukattil, C. Lovecchio, F. S. Cataliotti, F. Caruso, and A. Smerzi, Experimental realization of quantum Zeno dynamics, *Nat. Commun.* **5**, 3194 (2014).
- [67] P. Facchi and S. Pascazio, Quantum Zeno Subspaces, *Phys. Rev. Lett.* **89**, 080401 (2002).
- [68] F. Thiel, E. Barkai, and D. A. Kessler, First Detected Arrival of a Quantum Walker on an Infinite Line, *Phys. Rev. Lett.* **120**, 040502 (2018).
- [69] P. Kuklinski, Conditional probability distributions of finite absorbing quantum walks, *Phys. Rev. A* **101**, 032309 (2020).
- [70] F. Caruso, A. W. Chin, A. Datta, S. F. Huelga, and M. B. Plenio, Highly efficient energy excitation transfer in light-harvesting complexes: The fundamental role of noise-assisted transport, *J. Chem. Phys.* **131**, 105106 (2009).
- [71] D. A. Harville, *Matrix Algebra From a Statistician's Perspective* (Springer, New York, 2006).
- [72] R. Yin, K. Ziegler, F. Thiel, and E. Barkai, Large fluctuations of the first detected quantum return time, *Phys. Rev. Res.* **1**, 033086 (2019).
- [73] Q. Liu, R. Yin, K. Ziegler, and E. Barkai, Quantum walks: The mean first detected transition time, *Phys. Rev. Res.* **2**, 033113 (2020).
- [74] Y. Aharonov and J. Anandan, Phase Change During a Cyclic Quantum Evolution, *Phys. Rev. Lett.* **58**, 1593 (1987).
- [75] J. Anandan and Y. Aharonov, Geometric quantum phase and angles, *Phys. Rev. D* **38**, 1863 (1988).
- [76] V. Gebhart, K. Snizhko, T. Wellens, A. Buchleitner, A. Romito, and Y. Gefen, Topological transition in measurement-induced geometric phases, *Proc. Natl. Acad. Sci. USA* **117**, 5706 (2020).
- [77] K. Snizhko, P. Kumar, N. Rao, and Y. Gefen, Weak-Measurement-Induced Asymmetric Dephasing: Manifestation of Intrinsic Measurement Chirality, *Phys. Rev. Lett.* **127**, 170401 (2021).
- [78] K. Snizhko, N. Rao, P. Kumar, and Y. Gefen, Weak-measurement-induced phases and dephasing: broken symmetry of the geometric phase, *Phys. Rev. Res.* **3**, 043045 (2021).
- [79] Y. Wang, K. Snizhko, A. Romito, Y. Gefen, and K. Murch, Observing a Topological Transition in Weak-Measurement-Induced Geometric Phases, [arXiv:2102.05660](https://arxiv.org/abs/2102.05660).
- [80] M.-A. Miri and A. Alù, Exceptional points in optics and photonics, *Science* **363**, eaar7709 (2019).
- [81] K. B. Datta, *Matrix and Linear Algebra : Aided with Matlab*, Eastern Economy Condition (Prentice Hall, India, 2009).
- [82] D. C. Brody, Biorthogonal quantum mechanics, *J. Phys. A: Math. Theor.* **47**, 035305 (2014).
- [83] A. Ghatak and T. Das, New topological invariants in non-Hermitian systems, *J. Phys.: Condens. Matter* **31**, 263001 (2019).
- [84] A. M. Childs, E. Farhi, and S. Gutmann, An example of the difference between quantum and classical random walks, *Quantum Inf. Process.* **1**, 35 (2002).
- [85] S. R. Jackson, T. J. Khoo, and F. W. Strauch, Quantum walks on trees with disorder: Decay, diffusion, and localization, *Phys. Rev. A* **86**, 022335 (2012).

- [86] E. Farhi and S. Gutmann, Quantum computation and decision trees, *Phys. Rev. A* **58**, 915 (1998).
- [87] A. M. Childs, R. Cleve, E. Deotto, E. Farhi, S. Gutmann, and D. A. Spielman, Exponential algorithmic speedup by a quantum walk, in *Proceedings of the Thirty-Fifth Annual ACM Symposium on Theory of Computing* (Association for Computing Machinery, New York, 2003).
- [88] Z. Shi, H. Tang, Z. Feng, Y. Wang, Z. Li, J. Gao, Y. Chang, T. Wang, J. Dou, Z. Zhang, Z. Jiao, W. Zhou, and X. Jin, Quantum fast hitting on glued trees mapped on a photonic chip, *Optica* **7**, 613 (2020).
- [89] B. Misra and E. C. G. Sudarshan, The Zeno's paradox in quantum theory, *J. Math. Phys.* **18**, 756 (1977).
- [90] M. C. Fischer, B. Gutiérrez-Medina, and M. G. Raizen, Observation of the Quantum Zeno and Anti-Zeno Effects in an Unstable System, *Phys. Rev. Lett.* **87**, 040402 (2001).
- [91] H. Friedman, D. A. Kessler, and E. Barkai, Quantum walks: The first detected passage time problem, *Phys. Rev. E* **95**, 032141 (2017).
- [92] S. Lahiri and A. Dhar, Return to the origin problem for a particle on a one-dimensional lattice with quasi-Zeno dynamics, *Phys. Rev. A* **99**, 012101 (2019).
- [93] S. Belan and V. Parfenyev, Optimality and universality in quantum Zeno dynamics, *New J. Phys.* **22**, 073065 (2020).
- [94] V. Dubey, C. Bernardin, and A. Dhar, Quantum Dynamics under continuous projective measurements: non-Hermitian description and the continuous space limit, *Phys. Rev. A* **103**, 032221 (2021).
- [95] K. Snizhko, P. Kumar, and A. Romito, Quantum zeno effect appears in stages, *Phys. Rev. Res.* **2**, 033512 (2020).
- [96] F. Thiel and D. A. Kessler, Non-Hermitian and Zeno limit of quantum systems under rapid measurements, *Phys. Rev. A* **102**, 012218 (2020).